Three-body forces: From cold atoms to nuclei

Hans-Werner Hammer*

Helmholtz-Institut für Strahlen- und Kernphysik (Theorie)
and Bethe Center for Theoretical Physics,
Universität Bonn, D-53115 Bonn,
Germany

Andreas Nogga†

Institut für Kernphysik,
Institute for Advanced Simulation and Jülich Center for Hadron Physics,
Forschungszentrum Jülich, D-52425 Jülich,
Germany

Achim Schwenk‡

Institut für Kernphysik,
Technische Universität Darmstadt,
D-64289 Darmstadt, Germany
and ExtreMe Matter Institute EMMI,
GSI Helmholtzzentrum für Schwerionenforschung GmbH,
D-64291 Darmstadt,
Germany

arXiv:1210.4273v1 [nucl-th] 16 Oct 2012

It is often assumed that few- and many-body systems can be accurately described by considering only pairwise two-body interactions of the constituents. We illustrate that three- and higher-body forces enter naturally in effective field theories and are especially prominent in strongly interacting quantum systems. We focus on three-body forces and discuss examples from atomic and nuclear physics. In particular, we highlight the importance and the challenges of three-nucleon forces for nuclear structure and reactions, including applications to astrophysics and fundamental symmetries.

CONTENTS

I. Introduction 1

II. Theoretical approaches to three-body forces: definitions, dependence on scheme and framework 2

III. Universal aspects: From cold atoms to low-energy reactions and halo nuclei 4

IV. Three-body forces in few-nucleon systems 9

V. Three-nucleon forces and many-body systems 14

VI. Three-body forces and relations to other processes 18

VII. Outlook and future opportunities 20

Acknowledgments 22

References 22

I. INTRODUCTION

In this colloquium, we discuss recent advances, challenges, and perspectives of three-body forces in nuclear physics and related areas. We start with a brief overview of the history of the subject.

The simplest non-relativistic system in which three-body forces can appear is the three-body system. The study of the three-body problem has a long history in physics. The gravitational problem of the earth-moon-sun system was first considered by Newton (Newton (1687)). It was a central topic in mathematical physics from the mid 1700's to the early 1900's. In gravity, only two-body interactions between point masses are present. However, three-body tidal forces arise if extended objects, such as planets, are treated as point particles.

Three-body forces also play an important role in quantum mechanics and the quantum many-body problem. If they are not already present at a fundamental level, three- and higher-body forces appear in effective theories or in practical calculations, where the degrees of freedom and the Hilbert space have to be restricted. Typically, there is a hierarchy of these forces and two-body forces provide the main contribution with three- and higher-body forces giving smaller and smaller corrections.

A well known example of such a three-body force in nuclear physics is the Fujita-Miyazawa three-nucleon force (Fujita and Miyazawa (1957)). Its main contribution arises from the virtual excitation of a $\Delta(1232)$ resonance in processes involving three nucleons interacting

*hammer@hiskp.uni-bonn.de
†a.nogga@fz-juelich.de
‡schwenk@physik.tu-darmstadt.de

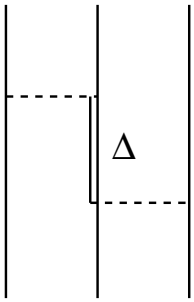

FIG. 1 Three-nucleon force arising from virtual excitation of a $\Delta(1232)$ degree of freedom. Solid (dashed) lines indicate nucleons (pions).

via pion exchanges illustrated in Fig. 1. In atomic, molecular and optical physics and quantum chemistry, non-additive forces arise if Born-Oppenheimer potentials are calculated by integrating out the electronic degrees of freedom (Kaplan and Novaro (1994)). In the theory of strong interactions, Quantum Chromodynamics (QCD), three-body forces arise already at a fundamental level as the three-gluon vertex induces an interaction between three quarks.

Our discussion here is guided by effective field theory ideas. The concept of *resolution* plays a key role in this context. In a scattering experiment, a particle beam with de Broglie wavelength λ can only probe structures at a scale $R \gtrsim \lambda$. Similarly, in a general process with typical momentum scale μ only physics at momenta $p \lesssim \mu$ (or, equivalently, distances $R \gtrsim 1/\mu$) is resolved. Effective theories and the renormalization group provide a method to use this observation for quantitative calculations. The resolution scale in an effective theory is controlled by the momentum cutoff Λ. Physics at momentum scales larger than the cutoff is excluded from the effective theory and encoded in effective couplings, so-called low-energy constants. These constants and the relative size of two- and higher-body forces turn out to be resolution dependent. If one starts with two-body forces only at high resolution, many-body forces will appear naturally as the resolution scale is lowered. These induced many-body forces capture the contributions of successive two-body interactions which are separated by a distance below the resolution scale.

The natural size of many-body forces is determined by the underlying scales of the theory and the external momentum scale μ. Effective field theories provide a convenient and systematic scheme to construct and estimate the size of many-body forces. It is one aim of this colloquium to exemplify these features. For example, chiral effective field theories in the Weinberg scheme have a clear hierarchy of many-nucleon forces. The current state of the art is to include two- and three-nucleon forces. In the future, however, the inclusion of four-body forces may also be required to achieve the desired accuracy.

The quantitative importance of three-body forces is well established in light nuclei. Therefore, they should contribute significantly in heavier nuclei as well. However, their inclusion in many-body calculations is computationally challenging and has only become feasible in recent years. We discuss three-nucleon forces at different resolution scales and show that their inclusion is mandatory for nuclear structure calculations. Whether this scheme breaks down for heavy nuclei beyond a certain mass number is an open question, but at present there are no indications of such a breakdown.

The outline of the colloquium is as follows: We start with a review of the theoretical framework for three-body forces including an illustration of their scheme dependence. In Section III, we discuss the role of three-body forces in the universal regime of large scattering-length systems and give examples from nuclear and cold atom physics. This is followed by a discussion of three-nucleon forces in chiral effective field theory in Section IV. The application of such forces to many-body systems and their relation to electroweak processes is presented in Sections V and VI. Finally, we give an outlook and discuss future opportunities.

II. THEORETICAL APPROACHES TO THREE-BODY FORCES: DEFINITIONS, DEPENDENCE ON SCHEME AND FRAMEWORK

Effective field theory (EFT) provides a general approach to understand the low-energy behavior of a physical system. The underlying principle was concisely formulated in Weinberg (1979): The most general Lagrangian consistent with all symmetries of the underlying interaction will generate the most general S-matrix consistent with these symmetries. If this idea is combined with a power counting scheme that specifies which terms are required at a desired accuracy, one obtains a predictive low-energy theory. The expansion is usually in powers of a low-momentum scale $M_{\rm low}$, which can be the typical external momentum, over a high-momentum scale $M_{\rm high}$. To illustrate this idea, consider a theory that is made of two particle species, a light and a heavy one with $M_{\rm low} \ll M_{\rm high}$. We focus on soft processes in which the energies and momenta are of the order of the light particle mass (the so-called soft scale). Under these conditions, the short-distance physics related to the heavy-particle exchange cannot be resolved. However, it can be represented systematically by contact interactions between light particles. Consider heavy-particle exchange between the light ones at momentum transfer $q^2 \ll M_{\rm high}^2$. The corresponding tree-level expression for the scattering amplitude is simply $g^2 r/(M_{\rm high}^2 - q^2)$ with g the heavy-light coupling constant. It can be expanded

in powers of $q^2/M_{\rm high}^2$ as:

$$\frac{g^2}{M_{\rm high}^2 - q^2} = \frac{g^2}{M_{\rm high}^2} + \frac{g^2\, q^2}{M_{\rm high}^4} + \dots \,. \tag{1}$$

This expansion can be represented in the EFT. At low momentum transfer q^2, the effects of the pole from the heavy-particle exchange in Eq. (1) are captured by a series of local momentum-dependent interaction terms reproducing the expansion in Eq. (1) term by term. This idea is closely related to the multipole expansion in classical electrodynamics and the renormalization group (Wilson (1983)).

The interactions in EFTs are represented by operators $\mathcal{O}_i$ that are monomials in the quantum fields ψ in the general interaction Lagrangian,

$$\mathcal{L}_{\rm int} = \sum_i g_i\, \mathcal{O}_i \,. \tag{2}$$

These operators can contain an arbitrary number of derivatives and/or fields but must respect the symmetries of the underlying theory. The derivatives are converted to momenta and generate the momentum dependence exemplified in Eq. (1). The coupling constants g_i can be ordered according to their importance at low energies from their scaling with $q \sim M_{\rm low}$ and $M_{\rm high}$. Operators with a larger number of derivatives or fields are usually suppressed. This is the basis of the power counting of the EFT.

An illustrative example is given by the Lagrangian

$$\mathcal{L}_{\rm int} = \sum_{i=2}^{N} g_i\, (\psi^\dagger\psi)^i \,, \tag{3}$$

which contains momentum-independent two-, three-, ... up to N-body contact interactions of a nonrelativistic field ψ. In a natural theory without any fine tuning of parameters, the dimensionful coupling constants g_i scale with powers of the high-momentum or breakdown scale $M_{\rm high}$. Dimensional analysis requires that $g_i \sim (1/M_{\rm high})^{3i-5}$, such that N-body interactions are suppressed by $(M_{\rm low}/M_{\rm high})^{2(N-2)}$ compared to $N-1$ successive two-body interactions (see, e.g., Hammer and Furnstahl (2000)). This type of scaling analysis is the basis of the suppression of many-body forces in the Weinberg scheme mentioned in the introduction.

The values of the coupling constants g_i are determined completely by on-energy-shell information, up to a well-defined truncation error. The exact relation, however, is not unique and depends on the renormalization scheme. In the construction of the most general Lagrangian, many-body forces arise naturally. These many-body forces have to be determined from many-body data.

A fundamental theorem of quantum field theory states that physical observables are independent of the choice of fields in a Lagrangian (Coleman *et al.* (1969); Haag (1958)). Consequently, they are invariant under redefinitions of the fields in the effective Lagrangian. Off-shell amplitudes, however, change under field redefinitions and thus are not observable. In systems with more than two nucleons, one can trade off-shell, two-body interactions for many-body forces.

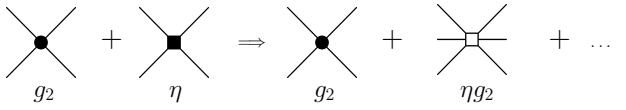

FIG. 2 Illustration of the field redefinition in Eq. (5) that trades an off-shell two-body interaction for a three-body interaction.

In a quantum mechanics framework, unitary transformations provide an alternative formalism to field redefinitions and lead to the same result (Amghar and Desplanques (1995); Polyzou and Glöckle (1990)). This explains how two-body interactions related by unitary transformations can predict different binding energies for the triton (Afnan and Serduke (1973)) if many-body forces are not consistently included.

We use a simple EFT model, to illustrate how field redefinitions can be used to shift strength from off-shell two-body interactions to on-shell three-body interactions (Hammer and Furnstahl (2000)):

$$\mathcal{L} = \psi^\dagger \mathcal{D}\psi - g_2(\psi^\dagger\psi)^2 - \eta\left(\psi^\dagger(\psi^\dagger\psi)\mathcal{D}\psi + \psi^\dagger\mathcal{D}(\psi^\dagger\psi)\psi\right) \,, \tag{4}$$

where $\mathcal{D} = i\partial_t + \vec{\nabla}^2/(2m)$ is the free Schrödinger operator. The model has a two-body contact interaction with coupling constant g_2 and an off-shell two-body contact interaction with coupling η which we assume to be small. Now consider a field transformation

$$\psi \longrightarrow \left[1 + \eta(\psi^\dagger\psi)\right]\psi \,, \quad \psi^\dagger \longrightarrow \left[1 + \eta(\psi^\dagger\psi)\right]\psi^\dagger \,. \tag{5}$$

Performing this transformation and keeping all terms of order η we obtain a new Lagrangian:

$$\mathcal{L}' = \psi^\dagger\mathcal{D}\psi - g_2(\psi^\dagger\psi)^2 - 4\eta g_2(\psi^\dagger\psi)^3 + \mathcal{O}(\eta^2) \,, \tag{6}$$

where the off-shell two-body interaction has been traded for a three-body interaction. This is illustrated in Fig. 2. Off-shell interactions always contribute together with many-body forces and only the sum of the two is meaningful. It is thus not possible to determine off-shell interactions from experiment.

On the other hand, if new interactions are generated from a given two-body interaction by field redefinitions or unitary transformations and only the two-body part is retained, many-body observables will depend on the interaction even if they generate the same two-body observables (see Furnstahl *et al.* (2001) for an explicit illustration in the above model). For example, nuclear

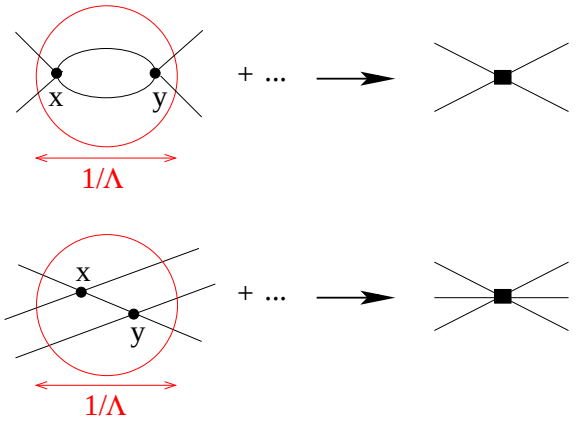

FIG. 3 Illustration for the resolution dependence of two- and three-body interactions.

matter binding curves will depend on the off-shell part of the two-body interaction, generating so-called "Coester bands" (Coester *et al.* (1970)). In the 1970s, it was proposed that comparisons of nuclear matter calculations could help to determine the "correct" off-shell behavior of the two-body interaction. From a modern perspective, it is clear that this is not possible and the bands will disappear if the full transformed Hamilitonian is used.

One might argue that it should be possible to find a suitable representation of the theory where three-body forces vanish or are very small. This strategy could be used to minimize the computational effort in many-body calculations. As discussed below, this is indeed possible for the universal EFT but only at leading order (LO). In theories with more complex operator structure and long-range interactions such as the chiral EFT, however, it is doomed to fail from the start. The various operators contribute differently to different observables and there is no optimal choice for removing the contributions of three-body forces at the same time for all observables.

As illustrated above, the interaction strength may be shifted from two- to many-body forces. This can also be seen by changing the momentum cutoff Λ in the regulators used in explicit calculations. Once the couplings g_i of the effective Lagrangian, the low-energy constants (LECs), have been adjusted to selected data, predictions for other low-energy observables should be independent of the choice for Λ. Obviously, this adjustment depends on Λ implying that also the interaction strengths of two- and many-body interactions vary with the cutoff and are not unique. The idea is illustrated in Fig. 3, where iterated two-body interactions at short-distance scales of $\sim 1/\Lambda$ are not resolved. Note that in practice the 3NFs generated in this way cannot be disentangled from the 3NFs at an initial scale, which will also have short-ranged (and other) contributions. It is therefore model-dependent to distinguish such "generated" from "genuine" 3NFs as is done often in the literature and, therefore, we will not distinguish 3NF mechanisms in this colloquium.

For two-body forces, this can be implemented by renormalization group (RG) equations for the potential (Bogner *et al.* (2007b, 2010))

$$\frac{d}{d\Lambda} V_\Lambda(12) = F(V_\Lambda, \Lambda)\,. \tag{7}$$

The RG equation describes the evolution with Λ of the matrix elements $V_\Lambda(12)$ of the potential in momentum space. The function F is defined such that the on-shell T-matrix is invariant under changes of the cutoff for momenta below Λ. This equation can be integrated from large Λ to lower cutoff scales. By construction, all two-body observables up to momenta of the order of the cutoff are invariant. Beyond this, e.g., for processes involving external probes and more particles, observables will depend on the cutoff. Complete RG invariance is only achieved when many-body forces and many-body currents are included. In principle, a similar RG equation for three- and higher-body interactions can be formulated. This has been realized in practice with the similarity RG (SRG) (Bogner *et al.* (2007a)) or by taking EFT three-nucleon forces (3NFs) as a general low-momentum basis (Nogga *et al.* (2004)), where the LECs are adjusted to few-nucleon data at the lower cutoffs. If the resolution scale Λ is not too low, the contributions of many-body forces obtained in this way are of the size expected in EFT and small compared to the two-nucleon (NN) force contributions, but they are still quantitatively important in state-of-the-art computations. The variation of the cutoff then enables one to estimate contributions of higher-body short-range interactions. This will be discussed in more detail in Section IV.

While the RG evolution is already an interesting tool to estimate many-body contributions to specific observables, it becomes even more valuable in many-body calculations (see Section V), where RG transformations to lower resolution lead to greatly enhanced convergence (Bogner *et al.* (2010)).

III. UNIVERSAL ASPECTS: FROM COLD ATOMS TO LOW-ENERGY REACTIONS AND HALO NUCLEI

As discussed in the previous section, the short-distance properties of a physical system are not resolved in low-energy observables. If no massless particles are present, all interactions appear short-ranged at sufficiently low energy. It is then possible to formulate an EFT with contact interactions.

Particularly interesting is the case of strong interactions characterized by a large scattering length a. Such systems are close to the unitary limit of infinite scattering length. It is obtained by taking the range of the interaction to zero while keeping a two-body bound state fixed

at zero energy.[1] In this limit, the two-body scattering amplitude is scale invariant and saturates the unitarity bound. Formulated as a challenge to test many-body methods (Bertsch (1999)), this limit turned out to be relevant for a variety of systems. It is historically interesting to note that an approximation corresponding to the unitary limit was already used in (Beth and Uhlenbeck (1937)) to calculate the second virial coefficient of a Fermi gas. Ultracold atomic gases can be tuned to the vicinity of the unitary limit using Feshbach resonances, while neutron matter is close to this limit through a fine tuning in nature. This gives rise to novel many-body phenomena, such as the BEC-BCS crossover in ultracold atoms (Giorgini *et al.* (2008)) and the "perfect" liquid observed in heavy-ion collisions (Schäfer and Teaney (2009)).

Here, we use the unitary limit as a starting point for an EFT expansion for strongly interacting quantum systems with short-range interactions. This universal EFT is applicable to any system close to the unitary limit, i.e., any system with short-range interactions and large scattering lengths. Examples include halo states in nuclear physics, ultracold atoms close to a Feshbach resonance, and hadronic molecules in particle physics. The breakdown scale $M_{\rm high}$ of this theory is set by the lowest energy degree-of-freedom not explicitly included in the theory. In nuclear and particle physics, this is typically given by one-pion exchange. In ultracold atoms, $M_{\rm high}$ is determined by the van der Waals interaction, but the details depend on the system. The typical momentum scale of the theory is $M_{\rm low} \sim 1/a \sim k$. For momenta k of the order of the breakdown scale $M_{\rm high}$ or above, the omitted short-range physics is resolved and has to be treated explicitly.

The universal EFT exploits the appearance of a large scattering length, independent of the mechanism generating it. Because the dependence of observables on the scattering length is explicit, it allows to unravel universal phenomena driven by the large scattering length such as universal correlations of observables (Phillips (1968), Tjon (1975)), the Efimov effect (Efimov (1970)), and limit-cycle physics (Braaten and Hammer (2003), Mohr *et al.* (2006)). For reviews of applications to the physics of ultracold atoms, see Braaten and Hammer (2006) and Platter (2009). The applications in nuclear and particle physics were discussed in Epelbaum *et al.* (2009a) and Hammer and Platter (2010).

Three-body forces play an important role in the universal EFT and we discuss their contribution in three- and higher-body systems in detail below. In the simplest case of spinless bosons, the leading-order Lagrangian can be written as:

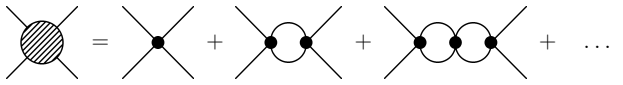

FIG. 4 The bubble diagrams with the contact interaction g_2 contributing to the two-body scattering amplitude.

$$\mathcal{L} = \psi^\dagger \Big(i\partial_t + \frac{\vec{\nabla}^2}{2m} \Big) \psi - g_2 (\psi^\dagger \psi)^2 - g_3 (\psi^\dagger \psi)^3 + \dots . \quad (8)$$

Extensions to more complicated systems are straightfoward. The terms proportional to g_2 and g_3 correspond to two- and three-body contact interactions. The dots represent higher-order terms suppressed by derivatives and/or more fields.

The renormalized values of the coupling constants g_2 and g_3 are matched to observables in the two- and three-body system. In the two-body system, one typically takes the S-wave scattering length. The exact relation between the coupling g_2 and the scattering length depends on the renormalization scheme. Because of this matching procedure, the EFT provides correlations between different observables based on the hierarchy of scales in the system. Given one set of observables, another set can be predicted to a certain accuracy. Depending on the experimental situation, these correlations can be applied in different ways.

Since the scattering length is large, $a \sim 1/M_{\rm low}$, the leading contact interaction g_2 has to be resummed to all orders (Kaplan *et al.* (1998); van Kolck (1999)). The two-body scattering amplitude is obtained by summing the bubble diagrams with the g_2 interaction shown in Fig. 4. This summation gives the exact solution of the Lippmann-Schwinger equation for the g_2 interaction and reproduces the leading term of the effective range expansion. Higher-order derivative interactions, which are not shown explicitly in Eq. (8), generate higher-order terms in the effective range expansion. Since these terms are set by $M_{\rm high}$, their contribution at low energies is suppressed by powers of $M_{\rm low}/M_{\rm high}$ and can be treated in perturbation theory. The first correction is given by the S-wave effective range, $r_0 \sim 1/M_{\rm high}$.

The S-wave scattering amplitude to next-to-leading order (NLO) then takes the form

$$T_2(k) = \frac{1}{-1/a - ik} \left[1 - \frac{r_0 k^2/2}{-1/a - ik} + \dots \right] , \quad (9)$$

where k is the relative momentum of the particles and the dots indicate corrections of order $(M_{\rm low}/M_{\rm high})^2$ for typical momenta $k \sim M_{\rm low}$. If a is large and positive, T_2 has a bound state pole at $k = i/a$. This corresponds to a two-body bound state (dimer) with binding energy $B_2 = 1/(2\mu a^2)$, where μ is the reduced mass of the particles. As $a \to \infty$, this bound state approaches the two-body threshold.

[1] In real physical systems the strict unitary limit of zero-range interactions can, of course, not be reached. In low-energy observables, however, the finite range R is not resolved and corrections are small (of the order of R/a or $R\,k$).

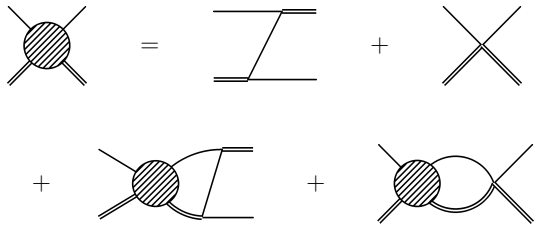

FIG. 5 The integral equation for the boson-dimer scattering amplitude. The single (double) line indicates the boson (dimer) propagator.

The universal EFT shows its full strength in the two-body sector when external currents are considered. In contrast to other approaches, the coupling to currents is straightforward and current conservation is satisfied at each stage of the calculation. Gauge-invariant few-body contact terms are generated naturally by writing the most general effective Lagrangian. Applications to a variety of electroweak processes in the two-nucleon sector have been carried out (see Beane *et al.* (2001); Bedaque and van Kolck (2002) for more details). Recently, these methods have also been applied to neutron-rich systems and halo nuclei. In Hammer and Phillips (2011), e.g., the electric properties of the one-neutron halo nucleus ^{11}Be were investigated. While this nucleus is nominally an 11-body system, the properties of its ground and first excited state can be described in the framework of the halo EFT (Bedaque *et al.* (2003a); Bertulani *et al.* (2002)). This EFT exploits the small binding energy of these two states compared to the typical energy scales of ^{10}Be (binding and excitation energies). Thus, ^{11}Be can be treated as an effective two-body system of the ^{10}Be core and a neutron. A similar strategy was applied to calculate the radiative neutron capture on a ^{7}Li core (Rupak and Higa (2011); Fernando *et al.* (2011)).

We now proceed to the three-body system where the term proportional to g_3 in Eq. (8) contributes. From naive dimensional analysis one would conclude that the g_3 term is of higher order (cf. discussion in Sec. II). This is indeed the case for two-component fermions where the Pauli principle forbids three fermions to be close together in an S-wave. In general, however, naive dimensional analysis fails for large scattering length a. Again, we focus on the case of identical bosons which already contains the main features of the problem. The simplest three-body process to be considered is the scattering of a boson and a dimer. The integral equation for boson-dimer scattering is shown schematically in Fig. 5. For total orbital angular momentum $L = 0$, it takes the form:

$$T_3(k,p;\,E) = \frac{16}{3a}\,M(k,p;\,E) + \frac{4}{\pi}\int_0^\Lambda dq\,q^2\,T_3(k,q;\,E) \times \frac{M(q,p;\,E)}{-1/a + \sqrt{3q^2/4 - mE - i\epsilon}}\,, \qquad (10)$$

where the inhomogeneous term reads

$$M(k,p;\,E) = \frac{1}{2kp}\ln\left(\frac{k^2+kp+p^2-mE}{k^2-kp+p^2-mE}\right) + \frac{H(\Lambda)}{\Lambda^2}\,, \qquad (11)$$

and a momentum cutoff Λ has been introduced to regulate the integral equation. All other three-body observables can be extracted from the amplitude T_3 taken in appropriate kinematics. In Eq. (10), H determines the strength of the three-body interaction $g_3(\Lambda) = -4m\,g_2(\Lambda)^2 H(\Lambda)/\Lambda^2$. The magnitude of the incoming (outgoing) relative momenta is k (p) and $E = 3k^2/(4m) - 1/(ma^2)$. The on-shell point corresponds to $k = p$ and the scattering phase shift can be obtained via $k\cot\delta = 1/T_3(k,k;\,E) + ik$.

For $H = 0$ and $\Lambda \to \infty$, Eq. (10) reduces to the STM equation first derived by Skorniakov and Ter-Martirosian (Skorniakov and Ter-Martirosian (1957)) which has no unique solution (Danilov (1961)). The regularized equation has a unique solution for any given (finite) value of the cutoff Λ but three-body observables show a strong dependence on the cutoff Λ. Cutoff independence of the amplitude is restored by an appropriate "running" of $H(\Lambda)$ which turns out to be a limit cycle (Bedaque *et al.* (1999a,b)):

$$H(\Lambda) \approx \frac{\cos[s_0\ln(\Lambda/\Lambda_*) + \arctan s_0]}{\cos[s_0\ln(\Lambda/\Lambda_*) - \arctan s_0]}\,, \qquad (12)$$

where $s_0 \approx 1.00624$ is a transcendental number and Λ_* is a dimensionful three-body parameter generated by dimensional transmutation. Adjusting Λ_* to a single three-body observable allows to determine all other low-energy properties of the three-body system. Note that the choice of the three-body parameter Λ_* is not unique and there are other definitions more directly related to experiment (Braaten and Hammer (2006)).

The physics of this renormalization procedure is illustrated in Fig. 6 where we show the unrenormalized three-body binding energies B_3 in the case of positive scattering length as a function of the cutoff Λ (solid line). As the cutoff is increased, B_3 increases. At a certain cutoff (indicated by the dotted line), a new bound state appears at the boson-dimer threshold. This pattern repeats every time the cutoff increases by the discrete scaling factor $\exp(\pi/s_0)$. Now assume that we adopt the renormalization condition that the shallowest state should have a constant energy given by the dashed line. At small values of the cutoff, we need an attractive three-body force to increase the binding energy of the shallowest state as

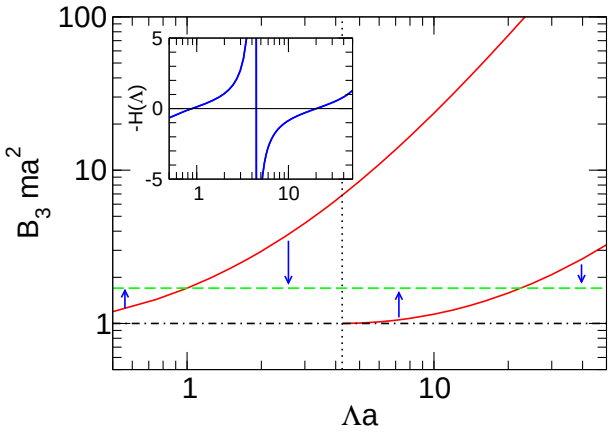

FIG. 6 (Color online) Unrenormalized three-body energies B_3 as a function of the momentum cutoff Λ (solid lines). The dotted line indicates the cutoff where a new three-body state appears at the boson-dimer threshold (dash-dotted line). The dashed line shows a hypothetical renormalized energy. The inset shows the running of the three-body force $g_3(\Lambda) \sim -H(\Lambda)$ with Λ.

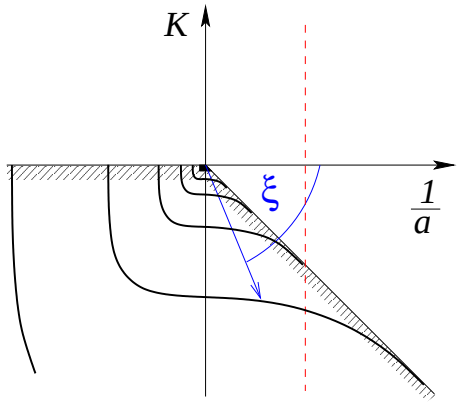

FIG. 7 (Color online) Illustration of the Efimov spectrum: The energy variable $K = \mathrm{sgn}(E)\sqrt{m|E|}$ is shown as a function of the inverse scattering length $1/a$. The solid lines indicate the Efimov states while the hashed areas give the scattering thresholds. The dashed vertical line indicates a system with fixed scattering length.

indicated by the arrow. As the cutoff is increased further, the required attractive contribution becomes smaller and around $\Lambda a = 1.1$ a repulsive three-body force is required (downward arrow). Around $\Lambda a = 4.25$, a new three-body state appears at threshold and we cannot satisfy the renormalization condition by keeping the first state at the required energy anymore. The number of bound states has changed and there is a new shallow state in the system. At this point the three-body force turns from repulsive to attractive to move the new state to the required energy. The corresponding running of the three-body force with the cutoff Λ is shown in the inset. After renormalization, the first state is still present as a deep state with large binding energy, but for threshold physics its presence can be ignored. This pattern goes on further and further as the cutoff is increased.

The three-body force in Eq. (12) has exactly the right behavior to implement the strategy from the previous paragraph. Moreover, it breaks the scale invariance in the unitary limit, because the three-body parameter Λ_* now provides a scale. However, due to the specific form of Eq. (12), a discrete scale invariance survives. Scaling transformations with the scaling factor $\lambda_0 = \exp(\pi/s_0)$ leave $H(\Lambda)$ and, consequently, three-body observables invariant. This discrete scaling symmetry is the signature of an RG limit cycle (Wilson (1971)). In the three-body bound-state spectrum it becomes manifest through the Efimov effect: The appearance of a geometric spectrum of three-body bound states (Efimov (1970)).

The Efimov spectrum is illustrated in Fig. 7. We show the energy variable $K = \mathrm{sign}(E)\sqrt{m|E|}$ as a function of the inverse scattering length $1/a$. The hashed areas indicate the three-atom ($a < 0$) and atom-dimer thresholds ($a > 0$) where the Efimov states become unstable. The spectrum is invariant under the discrete scaling transformations $K \to \lambda_0 K$ and $1/a \to \lambda_0/a$. As a consequence, there is an accumulation of Efimov three-body states at the origin. The scaling symmetry relates Efimov states along any ray with fixed angle ξ (cf. Fig. 7). In general, these states correspond to different scattering lengths. A physical system with fixed scattering length is illustrated by the vertical dashed line. For fixed a, the discrete scaling symmetry is only manifest in the unitary limit $1/a = 0$.

The parameter Λ_* can be used to set one of the three-body energies. All other states then follow from the discrete scaling symmetry. This explains why one parameter is sufficient for renormalization of the whole spectrum. The discrete scaling symmetry predicts infinitely-deep three-body states. This is known as the Thomas collapse (Thomas (1935)). Physically relevant, however, are only states with energies $|E| \ll M_{\mathrm{high}}^2/m$. All deeper states are ultraviolet artefacts of the effective theory and should be discarded.

The discrete scale invariance also manifests itself in the log-periodic dependence of scattering observables on the scattering length. This scaling behavior has been confirmed in cold atom experiments (Ferlaino and Grimm (2010)). In such experiments, the scattering length can be varied using Feshbach resonances. The scattering-length dependence of three-body recombination rates provides indirect information on the Efimov spectrum. For negative scattering length, the Efimov states hit the three-atom threshold, $E = 0$, for certain values of a (cf. Fig. 7) and lead to enhanced recombination rates. For positive scattering length, the Efimov states become unstable already at the atom-dimer threshold,

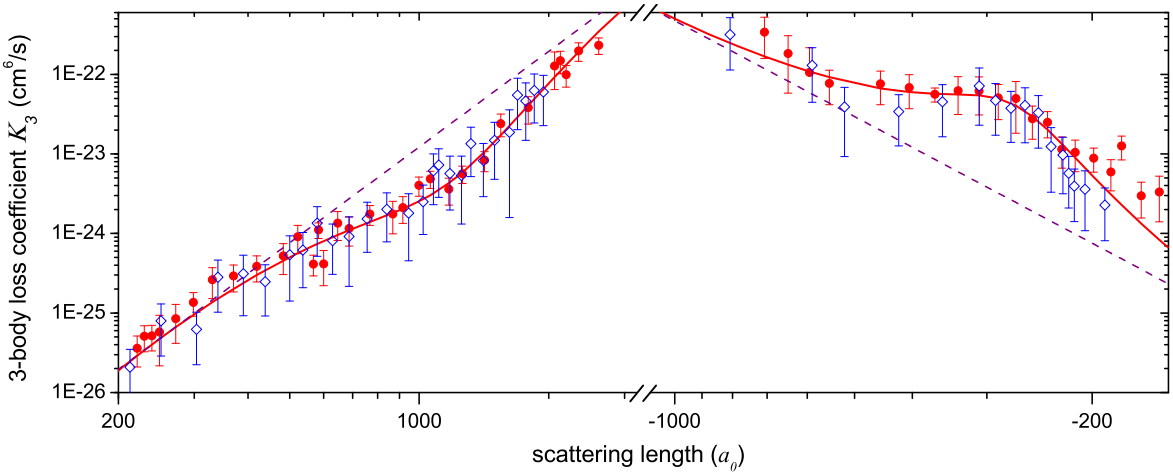

FIG. 8 (Color online) Three-body loss coefficient K_3 in a gas of ultracold ^{7}Li atoms as a function of scattering length (in units of the Bohr radius a_0) for the $|m_F = 1\rangle$ state (red solid circles) and the $|m_F = 0\rangle$ state (blue open diamonds). The solid lines represent fits to the universal EFT prediction. The dashed lines represent the $K_3 \sim a^4$ upper (lower) limit for $a > 0$ ($a < 0$). (Figure taken from Gross *et al.* (2010).)

$E = -1/(ma^2)$, but interference effects lead to minima and maxima in the rate at $E = 0$. Ideally one would like to see multiple recombination features on each side of the Feshbach resonance. For equal mass particles, this is not a simple task because of the large scaling factor. When effective-range effects are included perturbatively as in Eq. (9), the discrete scale invariance is softly broken, but the effects of the breaking on the recombination rate can be calculated (Ji *et al.* (2012)).

As an example, we show in Fig. 8 the three-body loss coefficient K_3 in a gas of ultracold ^{7}Li atoms measured by the Khaykovich group (Gross *et al.* (2010)) as a function of scattering length (in units of Bohr radius a_0) for the $|m_F = 1\rangle$ state (red solid circles) and the $|m_F = 0\rangle$ state (blue open diamonds). The data show that the positions and widths of recombination minima and Efimov resonances are identical for both states, which indicates that the short-range physics is nuclear-spin independent. The solid lines give fits to the analytical expressions of the universal EFT (Braaten and Hammer (2006)) and reproduce the data very well.

A more direct way to observe Efimov states is to populate these states directly through radio frequency transitions. This is difficult because of their short lifetime and has only recently been achieved for ^{6}Li atoms (Lompe *et al.* (2010); Nakajima *et al.* (2011)).

The integral equations for the three-nucleon problem are a generalization of Eq. (10). (For their explicit form and derivation, see Bedaque *et al.* (2003b).) The leading-order three-body force is required in all channels where short distances are not shielded by the angular momentum barrier and/or the Pauli principle. For S-wave nucleon-deuteron scattering in the spin-quartet channel the three-body force is of higher order, and the spin-quartet scattering phases can therefore be predicted to high precision from two-body data (Bedaque *et al.* (1998); Bedaque and van Kolck (1998)). In the spin-doublet channel there are two coupled channels but the renormalization is similar to the three identical-boson case. Thus, one needs a new parameter which is not determined in the NN system in order to determine the (leading) low-energy behavior of the three-nucleon system in this channel. A comprehensive discussion of three-body force effects in the three-nucleon system was given by Grießhammer (2005).

The three-body parameter gives a natural explanation of universal correlations between different three-body observables such as the Phillips line: a correlation between the triton binding energy and the spin-doublet neutron-deuteron scattering length (Phillips (1968)). These observables are calculated for different two-body potentials that reproduce the NN scattering phase shifts but the three-body parameter is not constrained by the data. This generates a one-parameter correlation between different three-body observables. These correlations are driven by the large scattering length and are independent of the mechanism responsible for it. As a consequence, they occur in atomic systems such as ^{4}He atoms as well (Braaten and Hammer (2006)). For an overview of this topic see Epelbaum *et al.* (2009a) and Hammer and Platter (2010).

The universal EFT has also been applied in the four-body sector. A study of the cutoff dependence of the four-body binding energies revealed that no four-body force is required for renormalization at leading order (Platter *et al.* (2004, 2005)). Thus, the four-body force is a higher-order effect. As a consequence, there are also universal correlations in the four-body sec-

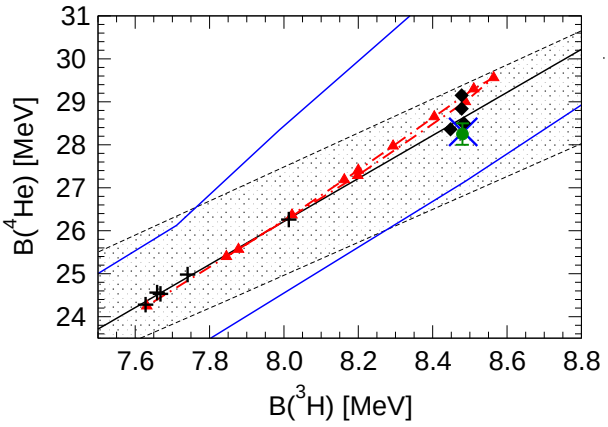

FIG. 9 (Color online) The Tjon line correlation between $B(^3\mathrm{H})$ and $B(^4\mathrm{He})$. The experimental value is shown by the cross. The shaded band gives the LO universal result (Platter *et al.* (2005)), while the outer solid lines include NLO corrections obtained using the resonating group method (Kirscher *et al.* (2010)). The pluses and diamonds show calculations using phenomenological NN and NN+3N potentials, respectively (Nogga *et al.* (2000)); the circle gives a chiral EFT result at $\mathrm{N^2LO}$ (Epelbaum *et al.* (2002)); and the triangles are based on an SRG-evolved $\mathrm{N^3LO}$ NN potential (Nogga *et al.* (2004); Hebeler *et al.* (2011)).

tor driven by the large scattering length. The prime example is the Tjon line (Tjon (1975)): a correlation between the triton and alpha-particle binding energies, $B(^3\mathrm{H})$ and $B(^4\mathrm{He})$. Higher-order range corrections break the correlation and generate a band. In Fig. 9, we show this band together with calculations using phenomenological NN potentials (Nogga *et al.* (2000)), a chiral NN potential at next-to-next-to-leading order ($\mathrm{N^2LO}$) (Epelbaum *et al.* (2002)), SRG-evolved next-to-next-to-next-to-leading order ($\mathrm{N^3LO}$) NN potentials (Nogga *et al.* (2004); Hebeler *et al.* (2011)), and the experimental value. All calculations with interactions that give a large scattering length must lie within the band. Different short-distance physics and/or cutoff dependence should only move the results along the band. This can be observed explicitly in the results for the SRG-evolved $\mathrm{N^3LO}$ NN potential indicated by the triangles in Fig. 9, as well as in few-body calculations with low-momentum interactions $V_{\mathrm{low}\,k}$ (Nogga *et al.* (2004)).

The absence of a four-body force at leading order also implies a universal four-body spectrum. In Hammer and Platter (2007) the dependence of the four-body bound-state spectrum on the two-body scattering length was investigated in detail and summarized in a generalized Efimov plot for the four-body spectrum. In particular, it was found that there are two four-body states tied to every Efimov trimer. In a subsequent study, von Stecher *et al.* (2009) extended these calculations to the four-particle threshold and confirmed the absence of a four-body parameter for shallow four-body states. Their prediction of the resonance positions lead to the experimental observation of universal tetramer states in ultracold caesium (Ferlaino *et al.* (2009)). This, in turn, has led to increased theoretical activity in this area. The sensitivity of tetramer energies to a four-body scale was, for example, investigated by Hadizadeh *et al.* (2011). Four-body recombination and other scattering processes were calculated by Deltuva (see Deltuva (2012) and references therein).

The bound-state properties of larger systems of bosons interacting through short-range interactions were considered by Hanna and Blume (2006). Using Monte Carlo methods they showed that universal correlations between binding energies can also be obtained. Calculations for larger number of particles using a model that incorporates the universal behavior of the three-body system were carried out by von Stecher (2010). These findings indicate that there is at least one N-body state tied to each Efimov trimer and numerical evidence was also found for a second excited 5-body state. In a subsequent study (von Stecher (2011)), the energies and structural properties of bosonic cluster states up to $N = 6$ were calculated for various two-body potentials. Besides the lowest cluster states, which behave as bosonic droplets, cluster states bound weakly to one or two atoms forming effective cluster-atom "dimers" and cluster-atom-atom "trimers" were identified. Thus the prospects for observing universal physics in larger few-body systems are excellent.

Recently, a geometric spectrum of universal three-body states has also been predicted for atoms with dipolar interactions (Wang *et al.* (2011)). In this case, the structure of the interaction is very similar to the nuclear tensor force generated by one-pion exchange. If the dipole moments of the atoms are aligned, the interaction is attractive in a head-to-tail configuration of the atoms and repulsive side-by-side, like for dipole magnets. If the dipole moments are anti-aligned, the interaction is opposite, repulsive and attractive, respectively. This might open the possibility to simulate the nuclear tensor force in experiments with ultracold atoms.

IV. THREE-BODY FORCES IN FEW-NUCLEON SYSTEMS

Three-body forces are especially important in nuclear physics. Phenomenological studies indicate, e.g., that the contribution of 3NFs to binding energies of light nuclei is quantitatively significant, of the order 20% (see Pieper and Wiringa (2001)).

In nuclear systems, the long-range parts of nuclear forces are mediated by pion exchanges in addition to short-range contact interactions discussed in the preceding section. The pion mass is comparable to the momenta

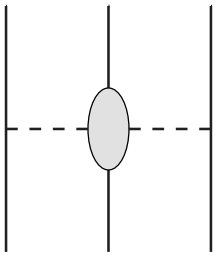

FIG. 10 Topology of the two-pion-exchange 3NF. Solid (dashed) lines indicate nucleons (pions).

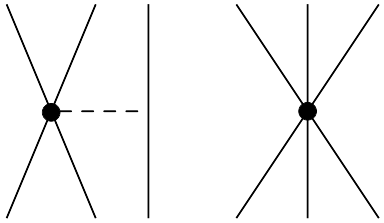

FIG. 11 Topology of the leading mid-range (left) and short-range (right) 3NFs. Solid (dashed) lines indicate nucleons (pions).

in typical nuclei. Therefore, it cannot be expected that pionless EFT is applicable, unless one considers very specific observables, e.g., for halo nuclei where the nucleon separation energy presents a low scale.

An important signature of 3NFs is the model dependence of few-nucleon predictions when only NN interactions are employed in the calculation. This is demonstrated by the ^{3}H and ^{4}He binding energies in Fig. 9. The model dependence indicates that the missing three-nucleon and higher-body interactions are different for each NN potential employed (Amghar and Desplanques (1995); Polyzou and Glöckle (1990)). Fortunately, 4N and higher-body forces are expected to be further suppressed. We will come back to this issue, but assume for the moment that such contributions are negligible.

It is therefore required to formulate both two- and three-body forces within one systematic scheme. Historically, this has not been the case. In most models, the main contribution is related to the two-pion-exchange contribution depicted in Fig. 10. Fujita and Miyazawa (1957) realized that this model can be constrained using pion-nucleon scattering data and found that the interaction is dominated by P-wave pion-nucleon (πN) interactions. This was the birth of modern 3NFs which were mostly developed independently of NN interactions (see, e.g., Coon *et al.* (1979)). Two-pion-exchange 3NFs are generally of the form (see Friar *et al.* (1999)):

$$V_{2\pi}^{\rm 3NF} = \frac{1}{2} \sum_{i\neq j\neq k} \frac{g_A^2}{(2f_\pi)^2} \frac{\vec{\sigma}_i \cdot \vec{q}_i \, \vec{\sigma}_j \cdot \vec{q}_j}{(\vec{q}_i{}^2 + m_\pi^2)(\vec{q}_j{}^2 + m_\pi^2)} F_{ijk}^{\alpha\beta} \tau_i^\alpha \tau_j^\beta \,, \tag{13}$$

with

$$F_{ijk}^{\alpha\beta} = \delta_{\alpha\beta} \left[-\frac{4c_1 m_\pi^2}{f_\pi^2} + \frac{2c_3}{f_\pi^2} \, \vec{q}_i \cdot \vec{q}_j \right] + \frac{c_4}{f_\pi^2} \, \epsilon^{\alpha\beta\gamma} \tau_k^\gamma \, \vec{\sigma}_k \cdot (\vec{q}_i \times \vec{q}_j) \,, \tag{14}$$

where i, j, k label particles and α, β, γ isospin, m_π is the pion mass, $f_\pi = 92.4\,$MeV the pion decay constant, and g_A the axial pion-nucleon coupling. The constants c_i are different for all models. In these equations, we have neglected cutoff functions that are required to regularize 3NFs at short distances.

In these models, the 3NFs are unrelated to the NN interaction, which shows up in a strong model dependence of predictions based on combining such 3NFs and different NN interactions. Although often parts of the parameters are adjusted using πN scattering data, one still needs to adjust a parameter of the 3NF, e.g., a cutoff parameter, such that the prediction for the ^{3}H binding energy agrees with experiment. Such combinations are not based on a consistent framework. They do not describe all available 3N scattering data, but they improve the description of many low-energy few-nucleon observables (Kalantar-Nayestanaki *et al.* (2012)). In part, this is related to the universal correlations of observables discussed in the last section. Such observables are thus not useful to pin down the spin-isospin structure of 3NFs.

Therefore, investigations have concentrated on intermediate-energy nucleon-deuteron scattering. Using phenomenological forces, it can be shown that, for this energy range, observables exist that are sensitive to the structure of 3NFs (Witała *et al.* (2001)). Due to a series of sophisticated nucleon-deuteron scattering experiments, data is now available (Kalantar-Nayestanaki *et al.* (2012)). Unfortunately, this data has not been analyzed yet in a framework that provides consistent NN and 3N interactions. Comparison of the data to the predictions based on phenomenological forces show that the current models do not describe the intermediate-energy data very well. We note that improvements of the models have been suggested (see, e.g., Kalantar-Nayestanaki *et al.* (2012) for more details). Here, we will focus on selected low-energy observables within a systematic approach to nuclear forces.

Such a systematic approach has been developed based on chiral EFT (for recent reviews, see Epelbaum (2006); Epelbaum *et al.* (2009a); Machleidt and Entem (2011)). Based on the symmetries of the QCD Lagrangian, most importantly its spontaneously broken chiral symmetry, it is possible to formulate an EFT in terms of nucleon degrees of freedom and the nearly massless Goldstone bosons of QCD: the pions. Symmetry considerations sufficiently constrain the interactions of pions with themselves and with nucleons to develop a systematic power counting scheme: chiral perturbation theory (ChPT).

The expansion parameter is Q/Λ_χ, where $Q \sim m_\pi$ is a typical momentum or the pion mass and $\Lambda_\chi \approx 1\,\mathrm{GeV}$ is the chiral-symmetry breaking scale. The terms of the Lagrangian that are relevant to our discussion here read

$$\begin{aligned}\mathcal{L} = \psi^\dagger \Bigg[& 4c_1 m_\pi^2 - \frac{2c_1}{f_\pi^2}\, m_\pi^2 \vec{\pi}^{\,2} + \frac{c_3}{f_\pi^2}\, \partial_\mu \vec{\pi} \cdot \partial^\mu \vec{\pi} \\ & - \frac{c_4}{2 f_\pi^2}\, \epsilon_{ijk}\, \epsilon_{abc}\, \sigma_i\, \tau_a\, (\nabla_j \pi_b)(\nabla_k \pi_c) \Bigg] \psi \\ & - \frac{D}{4 f_\pi} (\psi^\dagger \psi)(\psi^\dagger \vec{\sigma} \vec{\tau} \psi) \cdot \vec{\nabla} \pi \\ & - \frac{E}{2} (\psi^\dagger \psi)(\psi^\dagger \vec{\tau} \psi)(\psi^\dagger \vec{\tau} \psi) + \dots \,, \end{aligned} \tag{15}$$

where ψ and $\vec{\pi}$ are nucleon and pion fields, respectively. The Lagrangian includes as $\pi\pi$NN vertices the same LECs c_i of the two-pion-exchange 3NFs. In addition, these LECs also contribute to the subleading two-pion-exchange NN interaction, which shows the strong connection of NN and 3N forces.

The challenge for nuclear forces is that, because of bound state, parts of the interactions are nonperturbative in contrast to the interactions in pionic or πN systems. This issue has been tackled assuming that the power counting can be applied to all non-reducible diagrams without purely nucleonic intermediate states. These diagrams form a potential that is then summed to all orders solving the Schrödinger equation (Weinberg (1990)). The approach requires numerical regularization of the potential introducing a regulator dependence. In state-of-the-art applications, cutoffs are presently restricted to values $\Lambda \lesssim 450 - 600\,\mathrm{MeV}$. There is a lively discussion whether this constraint is an artifact and can be overcome by an improved power counting, or whether it is an inherent requirement of a nonperturbative extension of ChPT (Epelbaum and Gegelia (2009); Hammer *et al.* (2007); Nogga *et al.* (2005); Valderrama (2011)). For applications to many-nucleon systems, lower cutoffs are advantageous and in some cases, computations are only feasible with lower cutoffs. For the estimate of missing higher-order contributions, we will assume a high scale $\Lambda_\chi \approx \Lambda$ in this section.

In chiral EFT, NN, 3N and higher-body forces can be derived consistently. The general result is that higher-body forces are suppressed compared to lower-body ones. This justifies our assumption that 4N and higher-body forces are further suppressed. For NN interactions, one finds that the longest-range part is one-pion exchange, which is also the basis of state-of-the-art NN models. The first 3NF contribution is suppressed by $(Q/\Lambda_\chi)^3$ (van Kolck (1994)) and contains the two-pion-exchange part given by Eq. (13). At the same order of the expansion, two other topologies (see Fig. 11) contribute

$$V_{\mathrm{short}}^{\mathrm{3NF}} = \sum_{i \neq j \neq k} \left[-D\, \frac{g_A}{8 f_\pi^2}\, \frac{\vec{\sigma}_j \cdot \vec{q}_j\, \vec{\sigma}_i \cdot \vec{q}_j}{\vec{q}_j^{\,2} + m_\pi^2}\, \vec{\tau}_i \cdot \vec{\tau}_j + \frac{E}{2}\, \vec{\tau}_j \cdot \vec{\tau}_k \right]. \tag{16}$$

Usually, these parts are called the D- and E-term. The D-term is of mid range (one-pion-exchange–short-range) and the E-term is of short range. This implies that the E-term coupling can only be obtained from few-nucleon observables, whereas the D-term strength is also related to weak or pionic processes involving two nucleons (see Section VI). Following standard conventions, we introduce two dimensionless couplings $c_D = D\, f_\pi^2 \Lambda_\chi$ and $c_E = E\, f_\pi^4 \Lambda_\chi$. As noted above, due to the c_i vertices of the Lagrangian, ChPT provides relations between the strength of the two-pion-exchange NN interaction and $V_{2\pi}^{\mathrm{3NF}}$. This level of consistency can only be implemented in the framework of ChPT. For the results given here, the Δ is not treated as an explicit degree of freedom. Since the mass difference of the nucleon and the Δ is only $\sim 2m_\pi$, an explicit inclusion is expected to improve the convergence of the chiral expansion (Kaiser *et al.* (1998); Krebs *et al.* (2007); Ordóñez *et al.* (1994)). For 3NFs, the leading Δ contribution is entirely included in $V_{2\pi}^{\mathrm{3NF}}$ and shows up in larger strength constants c_3 and c_4 enhancing the two-pion-exchange contributions compared to the other two topologies (Epelbaum *et al.* (2008)).

In nuclear systems the separation of the high and the low scales (given by Λ and the pion mass or a typical momentum of the system, respectively) is not exceedingly large, which implies a slowly converging chiral expansion. Especially for intermediate-energy nucleon-deuteron scattering, the expansion parameter is estimated to be $\sim 1/2$ or larger. Therefore, calculations up to order Q^3 (including the leading 3NFs) are useful only up to nucleon laboratory energies of $\sim 100\,\mathrm{MeV}$. Fortunately, the Q^4 3NF contributions have been completed recently (Bernard *et al.* (2008, 2011)), and applications are under way.

Before calculations based on chiral 3NFs can be performed, one needs to determine the LECs c_i, c_D and c_E. The c_i constants have been determined from NN data as well as πN data. The results are summarized in Table I. For simplicity, we have omitted the theoretical uncertainties and only give the central values. Most determinations are in agreement within the uncertainties, but deviations of the different determinations can be sizable, of the order of 30%. For our purpose here, this accuracy is sufficient and comparable to higher-order contributions that we do not take into account. This problem will become more relevant, when the subleading parts of the 3NF will allow us to increase the accuracy of our predictions. In principle, these constants can be obtained independently of the NN interaction. So their size should not depend on the regulator chosen or on the specific realization of chiral NN potentials.

TABLE I Comparison of different c_i determinations. The c_i's are given in GeV^{-1}. At present, the determinations using NN observables require further constraints from πN observables to be conclusive. The last column indicates whether the c_i values are mostly based on NN or πN data. We also show the results based on resonance saturation (res) from Bernard *et al.* (1997) (note that we omitted the πN fit from that paper).

	c_1	c_3	c_4	
Fettes *et al.* (1998) (Fit 1)	-1.2	-5.9	3.5	πN
Büttiker and Meißner (2000)	-0.8	-4.7	3.4	πN
Meißner (2007)	-0.9	-4.7	3.5	πN
Rentmeester *et al.* (2003)	-0.8	-4.8	4.0	NN
Entem and Machleidt (2002)	-0.8	-3.4	3.4	NN
Entem and Machleidt (2003)	-0.8	-3.2	5.4	NN
Epelbaum *et al.* (2005)	-0.8	-3.4	3.4	NN
Bernard *et al.* (1997)	-0.9	-5.3	3.7	res

Based on naturalness arguments, one would expect that the c_i's are of the order of $\Lambda_\chi^{-1} \sim 1\,\mathrm{Gev}^{-1}$. It sticks out that c_3 and c_4 are larger than this estimate. This can be understood based on resonance saturation, where the large c_i's are related to the small Δ to nucleon mass difference $\sim 1/(m_\Delta - m)$ (see, e.g., Bernard *et al.* (1997)). Taking Δ's explicitly into account reduces the magnitude of the c_i considerably so that an improved convergence of the chiral expansion can then be expected (see Section VII and Krebs *et al.* (2007) in the context of NN interactions).

Finally, we need to determine the constants c_D and c_E. Usually, combinations of c_D and c_E are found that make sure that the ^{3}H binding energy is described correctly. Then different strategies have been used to constrain c_D from few-nucleon data, e.g., by fitting the doublet neutron-deuteron scattering length (Epelbaum *et al.* (2002)), the binding energy of ^{4}He (Nogga *et al.* (2006)), or the radius of ^{4}He (Navrátil *et al.* (2007)). In addition, the ^{3}H beta decay half-life can be used to constrain c_D (see Section VI). In particular, the fit of c_D to the ^{3}H beta decay half-life or to the radius of ^{4}He have been shown to lead to a good overall description of light and p-shell nuclei. It is important to note that many low-energy observables are already well described once c_D and c_E combinations have been chosen that describe the ^{3}H binding energy correctly. Therefore, the sensitivity of these observables on c_D is low and a considerable uncertainty remains. Possibly, for higher-order calculations, other strategies need to be devised to obtain more accurate determinations of c_D and c_E.

Since the separation of scales is not very large and since there are ongoing discussions on the size of the high scale for nuclei, it is instructive to calculate the contributions of NN and 3N forces to the binding energy of light nuclei. These contributions are not observables, nevertheless their relative size can be estimated and compared to the power counting estimate. For this estimate, we use the realization of chiral EFT interactions at order Q^3 of Epelbaum *et al.* (2005) (with $\tilde{\Lambda} = 700$ MeV). In this work, the NN potential has been fitted for different cutoffs, which can be used to investigate the scale dependence of chiral 3NFs. For the 3NF, we use the same c_i values as for the NN part. The c_D and c_E values have been determined by a fit to the ^{3}H binding energy and the doublet neutron-deuteron scattering length. The chiral 3NFs have been regularized using a cutoff function depending on the relative momenta in the in- and outgoing state where the cutoff is identical to the Λ of Epelbaum *et al.* (2005). The results are given in Table II. As one can see, the binding energy of ^{4}He is close to the experimental value of 28.30 MeV. The remaining deviation from experiment is comparable to the cutoff dependence and indicates the contribution that can be expected from order Q^4. The leading 3NF is a Q^3 contribution. Assuming a typical momentum $\sim m_\pi$ and $\Lambda_\chi = 500\,\mathrm{MeV}$, we expect a contribution of approximately 2% to the potential energy. It is apparent that the contribution of 3NFs strongly depends on the cutoff. For the first case in Table II, the size is smaller than expected, which is no contradiction to the power counting. For the second case, the 3NF contribution is somewhat larger than naively expected. The estimate is still within a factor of $3-4$ correct (a natural-sized number), but it shows the enhancement of the 3NF due to the Δ resonance.

TABLE II Power counting predictions and explicit results for the binding energy B and the expectation values of NN and 3N forces for ^{4}He. Cutoffs and energies are given in MeV.

Λ	B	$\langle V_{\mathrm{NN}}\rangle$	$\langle V_{\mathrm{3NF}}\rangle$	$\left\lvert\frac{\langle V_{\mathrm{3NF}}\rangle}{\langle V_{\mathrm{NN}}\rangle}\right\rvert$ [%]
450	27.65	-84.56	-1.11	1.3
600	28.57	-93.73	-6.83	7.2

In summary, the overall size of 3NF contributions is as expected from the power counting once the contribution of the Δ resonance has been taken into account. The deviation of the binding energy for ^{4}He can also be expected from a higher-order contribution. On a quantitative level, this deviation indicates that high precision can only be expected for a Q^4 calculation.

At order Q^3, there are also nucleon-deuteron scattering calculations available. At intermediate energies, the results are strongly dependent on the cutoff. For low energy, however, many observables can be accurately predicted. In the left panel of Fig. 12, we show as an example the elastic nucleon-deuteron cross section. For the elastic cross section, data and prediction are in excellent agreement, and the order Q^2 and Q^3 results are similar indicating that the calculation is converged with respect

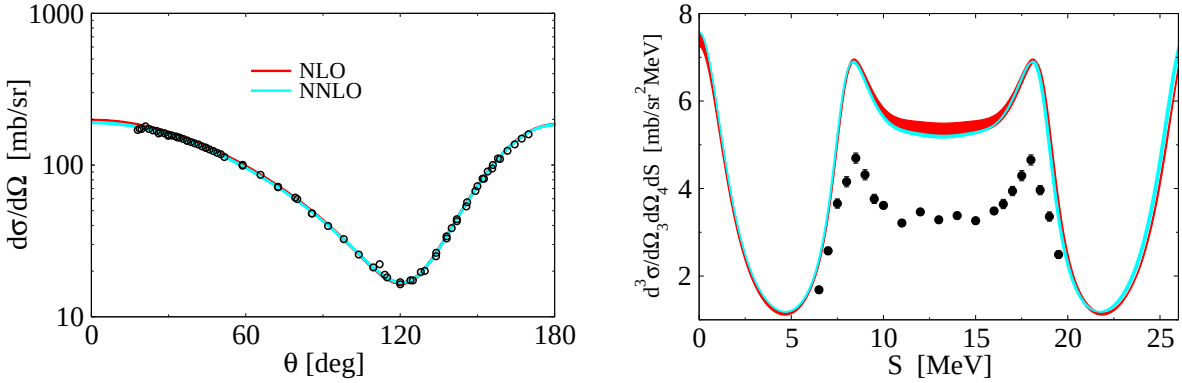

FIG. 12 (Color online) Left panel: Elastic nucleon-deuteron cross section at 10 MeV. The almost indistinguishable bands correspond to chiral Q^2 (red, dark grey) and Q^3 (cyan, light grey) calculations. Data are from Howell *et al.* (1987); Rauprich *et al.* (1988); Sagara *et al.* (1994); Sperisen *et al.* (1984). Right panel: Nucleon-deuteron breakup cross section at 19 MeV for the space-star configuration at $\alpha = 56°$ (see Ley *et al.* (2006) for the definition of the kinematics). The bands are the same as in the left panel. The data is from Ley *et al.* (2006).

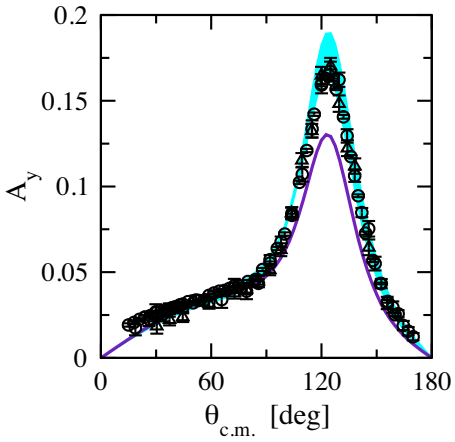

FIG. 13 (Color online) The nucleon vector analyzing power A_y for elastic nucleon-deuteron scattering at 10 MeV. The cyan band covers predictions based on chiral NN and 3N forces at order Q^3 for various cutoffs. The solid, purple line is the result of the CD-Bonn NN combined with the TM99 3N potential. Data as in the left panel of Fig. 12. Reprinted with permission from Kalantar-Nayestanaki *et al.* (2012).

to the chiral expansion. Whereas the bulk of the observables at low energies are nicely reproduced, there are a some exceptions. One of them is a specific breakup configuration shown in the right panel of Fig. 12. Again, the Q^2 and Q^3 results nicely agree indicating convergence of the chiral expansion and, therefore, small contributions of 3NFs. Unfortunately, there is a large discrepancy to the data. This is still an unresolved problem.

A different example is the analyzing power at low energy shown in Fig. 13. The solid line represents the result based on high-precision phenomenological forces, which clearly disagrees with the data. This is a common feature of all available calculations based on phenomenological forces and has been discussed vividly in the literature (see, e.g., Miller and Schwenk (2007)). At order Q^3, for the realization of Epelbaum *et al.* (2005), the result seems to agree with the data. However, the cutoff dependence is unusually large for these small energies and a detailed analysis reveals that this agreement in the three-body sector can be traced back to deficiencies in the description of NN data. Therefore, at order Q^3, the analyzing power cannot be properly predicted but is merely accidentally described. We stress that the analyzing power is a very small observable, so that tiny improvements of the Hamiltonian can be relevant for a proper prediction. This is in line with the rather strong dependence on the cutoff, which indicates that order Q^4 contributions might resolve this puzzle. For the 4N system, a more significant deviation of data and predictions of the analyzing power has been found by Viviani *et al.* (2001). Interestingly, in this case, chiral 3NFs lead to an improved description of the data compared to the standard phenomenological forces (Viviani *et al.* (2010)).

In summary, the results for few-nucleon systems show that Q^3 predictions are in line with the expectations based on power counting. Whereas low-energy scattering is reasonably described at this order, the results for the binding energies indicate that Q^4 will be required to reach satisfactory accuracies. Two-nucleon forces at this order are available and have an accuracy comparable to phenomenological forces (Entem and Machleidt (2003); Epelbaum *et al.* (2005)). The 3NFs at N^{3}LO have been completed recently (Bernard *et al.* (2008, 2011)). In addition, a consistent calculation up to this order also involves 4N forces, which fortunately do not involve additional LECs and are therefore parameter free. They have been derived and explored in ^{4}He (Epelbaum (2007); Nogga *et al.* (2010)). In this case, for the small cutoffs, the contributions seems to be smaller than expected. It

remains to be seen whether this is also true for more complex systems.

Next, we return to the discussion of the RG transformation started in Section II, because the resolution scale dependence also applies to the low-energy couplings in 3NFs. Therefore, the RG equation in the NN sector, Eq. (7) needs to be augmented by a similar equation for 3NFs, which we again write schematically as

$$\frac{d}{d\Lambda} V_\Lambda(123) = F_{123}(V_\Lambda(ij), V_\Lambda(123), \Lambda)\,. \qquad (17)$$

For low-momentum interactions $V_{\mathrm{low}\,k}$, solving the RG equation for 3NFs is difficult in practice, because it involves a complete set of scattering solutions for the three-body system (Bogner *et al.* (2010)). This is not feasible at this point, but a consistent 3NF evolution can be carried out in the SRG approach (as discussed below). For low-momentum interactions, the chiral EFT has been used as a general operator basis of 3NFs, and the LECs have been adjusted directly to few-nucleon data at lower resolution scales (Hebeler *et al.* (2011); Nogga *et al.* (2004)). Such an approach is justified for $\Lambda \lesssim 500\,\mathrm{MeV}$, because the NN interactions become universal (Bogner *et al.* (2003)). It is therefore motivated that consistent 3NFs should have the same form as the ones derived in chiral EFT. Since 3NFs are defined up to a finite order, even three-nucleon observables will only be approximately independent of the cutoff. It is therefore common to perform calculations for a range of cutoff values. The variation of the prediction provides an estimate of the theoretical uncertainty due to neglected higher-order 3NFs. If observables are calculated for more complex systems, the dependence on the cutoff can also be due to neglected four- and higher-body interactions.

The SRG approach provides a powerful scheme to evolve 3NFs by differential equations of the general form of Eqs. (7) and (17). The SRG transformation is an exact unitary transformation. Therefore, all NN observables are invariant under the transformation. By construction, low and high momenta decouple, and observables at low momentum becomes insensitive to high-momentum details (Jurgenson *et al.* (2008)). As a result, many-body calculations converge more rapidly for evolved potentials, similar to low-momentum interactions. The SRG evolution of 3NFs has been achieved in a harmonic-oscillator basis (Jurgenson *et al.* (2009); Roth *et al.* (2011)) and recently in momentum space (Hebeler (2012)).

The results of the application of SRG-evolved NN and 3N interactions to ^{4}He again shows the quantitative importance of 3NFs for binding energies of nuclei. But it also supports the general belief that four-nucleon forces do not contribute significantly, as shown in Fig. 14. When the SRG flow is truncated at the two-body level, the ground-state energy of ^{4}He depends significantly on the SRG flow parameter λ, which plays a similar role as the momentum cutoff Λ. However, the λ variation

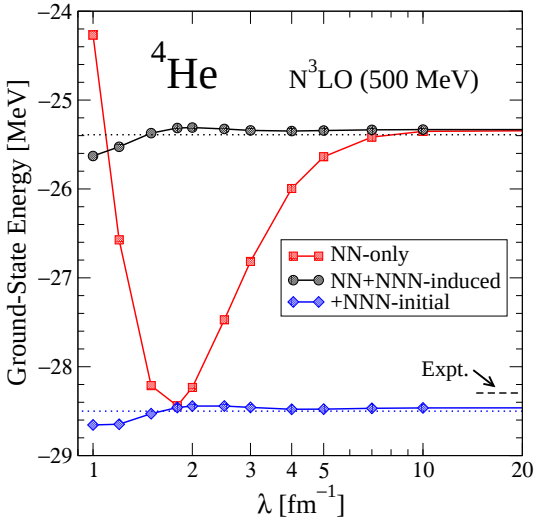

FIG. 14 (Color online) Ground-state energy of ^{4}He as a function of the SRG flow parameter λ starting from chiral NN and 3N interactions at N^{3}LO and N^{2}LO, respectively. For details see Jurgenson *et al.* (2009).

is of the same order as the 3NF contribution. This shows how the RG/SRG cutoff variation estimates missing parts of the Hamiltonian. When 3NFs are included in the SRG evolution, most of the λ dependence is removed. The remaining variation is of the order of 50 keV for $\lambda \gtrsim 1.5\ \mathrm{fm}^{-1}$, indicating that induced 4N forces provide a small contribution to the ^{4}He ground-state energy. Note that this estimate is even smaller than explicit calculations using 4N forces (Deltuva *et al.* (2008); Nogga *et al.* (2010)), which result in $200 - 300$ keV for ^{4}He.

The small size of 4N forces justifies the exploration of larger nuclei and nuclear matter based on chiral NN and 3N interactions in the next Section. The detailed calculation of 4N forces indicates that the result for ^{4}He might be suppressed because parts of the force cancel for these quantum numbers. Eventually, this result needs to be confirmed for more complex systems than ^{4}He.

V. THREE-NUCLEON FORCES AND MANY-BODY SYSTEMS

Three-body forces are a frontier for understanding and predicting strongly interacting many-body systems. While the quantitative importance of 3NFs has been well established in light nuclei, they are currently not included in most nuclear structure calculations. In this section, we discuss the opportunities and challenges this area offers. We highlight the importance of 3NFs beyond light nuclei, for neutron-rich systems, and for nucleonic matter in astrophysics, with a focus on 3NFs based on chiral EFT. Although some of the applications that we discuss

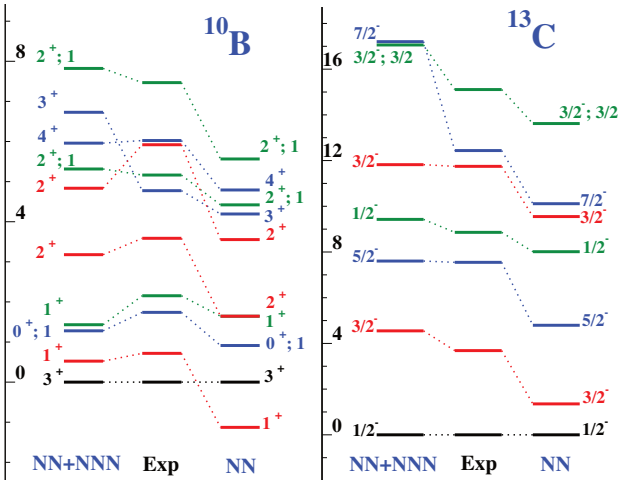

FIG. 15 (Color online) Excitation energies in MeV of light nuclei, ^{10}B and ^{13}C, obtained in the ab-initio No-Core Shell Model (NCSM) with chiral EFT interactions (NN to N^{3}LO and 3N to N^{2}LO) (Navrátil *et al.* (2007)).

still require an approximative treatment of 3NFs, they exhibit new facets and significant contributions of 3NFs.

As discussed in the previous section, chiral EFT opens up a systematic path to investigate many-body forces, which has not been possible before. This results from the consistency of NN and 3N interactions and the possibility to constrain all parameters using only few-nucleon data. No new parameters enter for 3N and 4N forces at N^{3}LO. Moreover, it has been shown that for systems of only neutrons, the D and E parts do not contribute because of the Pauli principle and the coupling of pions to spin (Hebeler and Schwenk (2010); Tolos *et al.* (2008)). This establishes a forefront connection of the investigation of 3NFs with the exploration of neutron-rich nuclei at rare isotope beam facilities worldwide.

As expected from the Tjon band in Fig. 9, 3NFs impact binding energies and therefore also radii. Precision techniques for masses and charge radii present new challenges for theory (in the context of 3NFs see, e.g., Brodeur *et al.* (2012)). In addition, similar to the spin dependences observed in few-body scattering, e.g., for the analyzing power A_y discussed in Fig. 13, 3NFs play an important role for spin-orbit splittings and spin dependences in nuclei. Both aspects can be clearly seen in the spectra of light nuclei, where calculations can be performed ab-initio, making these nuclei an interesting laboratory to explore nuclear forces. As an example, we show two representative spectra in Fig. 15, calculated in the No-Core Shell Model (NCSM) including chiral 3NFs at N^{2}LO (Navrátil *et al.* (2007)). The NCSM is based on a large-basis Hamiltonian diagonalization. Without 3NFs the spectra are generally too compressed (which is also found for ^{23}O in Fig. 16 and for other medium-mass nuclei). Clearly, the spectrum improves, when 3NFs are taken into account. In addition to a repulsive effect on the spectra, 3NFs provide important contributions to the spin-orbit splitting, reflected in the excitation energy of the first $^3/_2^-$ state relative to the $^1/_2^-$ ground state in ^{13}C, which probes the splitting of the $p_{3/2} - p_{1/2}$ orbitals. This can also be seen in the 3NF contributions to the spin-orbit splitting between the $p_{1/2}$ and $p_{3/2}$ phase shifts in nucleon-^{4}He scattering (Nollett *et al.* (2007)). For ^{10}B, NN forces alone do not predict the correct ground-state spin and parity 3^+, but instead the lowest state is found to be 1^+. This is only corrected by some of the phenomenological 3NFs (Pieper (2008)). For chiral 3NFs, the correct ordering is predicted. This is also needed for the analogous states in medium-mass nuclei ^{22}Na and ^{46}V, which are $N = Z = 8$ and $N = Z = 20$ nuclei with three valence neutrons and three valence protons (Nowacki (2008)). Moreover, recent work has demonstrated the impact of 3NFs on the structure probed in electroweak transitions (see also Section VI), e.g., for the beta decay of ^{14}C used for carbon dating (Holt *et al.* (2009); Maris *et al.* (2011)).

Nuclear lattice simulations were recently used to perform the first ab-initio calculation of the Hoyle state in ^{12}C (Epelbaum *et al.* (2011)), which is important for nucleosynthesis. Due to its alpha-cluster structure, this state is challenging for many-body methods. In this approach, spacetime is discretized and the nucleons are located on the lattice sites. Their interactions in chiral EFT are implemented using auxiliary fields and the low-lying states are extracted using a generalized Euclidean time projection method. This promising new method allows to take 3NFs into account without handling large interaction matrices.

The application of RG transformations to evolve nuclear forces to lower resolution leads to greatly enhanced convergence in few- and many-body systems (Bogner *et al.* (2010)). Current research focuses on extending these methods to 3NFs using the SRG. This has been achieved in a harmonic-oscillator basis (Jurgenson *et al.* (2009); see Fig. 14), with promising results in light and medium-mass nuclei in the NCSM and importance-truncated NCSM (Jurgenson *et al.* (2011); Roth *et al.* (2011)), and recently in momentum space (Hebeler (2012)). Open questions include understanding the cutoff dependence in chiral EFT, whether long-range many-body interactions are induced by the SRG, and to explore the dependence on the SRG generator.

Three-nucleon forces have also been implemented for neutron-rich systems. A frontier in this area is to understand the sequence of isotopes from proton-rich to the limit of neutron-rich nuclei: the neutron dripline. The neutron dripline evolves regularly from light to medium-mass nuclei except for a striking anomaly in the oxygen isotopes (Otsuka *et al.* (2009)), where the heaviest isotope, ^{24}O, is doubly-magic and anomalously close to stable nuclei (Janssens (2009) and references therein).

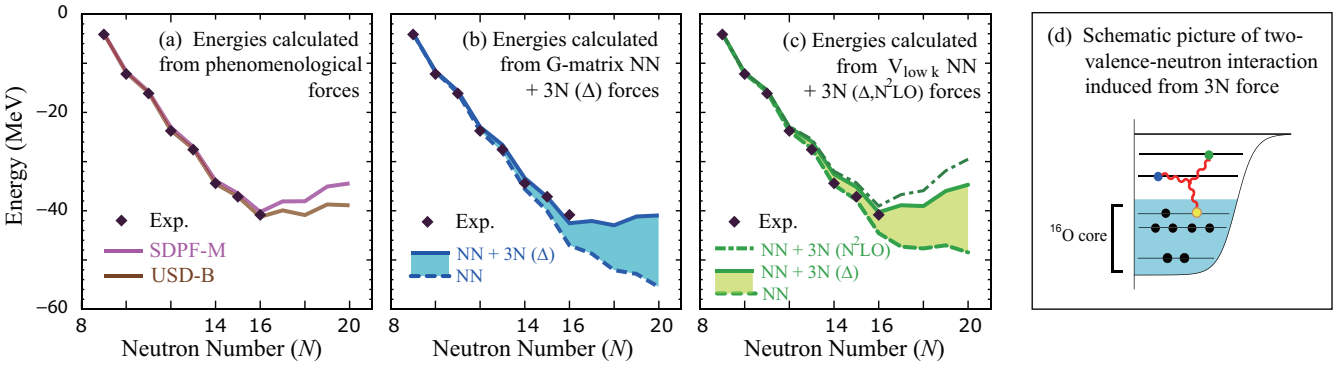

FIG. 16 (Color online) Ground-state energies of the neutron-rich oxygen isotopes relative to ^{16}O, including experimental values of the bound isotopes $^{16-24}$O. Energies obtained from (a) phenomenological forces SDPF-M and USD-B, (b) a G matrix interaction and including Fujita-Miyazawa 3NFs due to Δ excitations, and (c) from low-momentum interactions $V_{\mathrm{low}\,k}$ and including chiral 3NFs at N^{2}LO as well as only due to Δ excitations. The changes due to 3NFs based on Δ excitations are highlighted by the shaded areas. (d) Schematic illustration of a two-valence-neutron interaction generated by 3NFs with a nucleon in the ^{16}O core. For details see Otsuka *et al.* (2009).

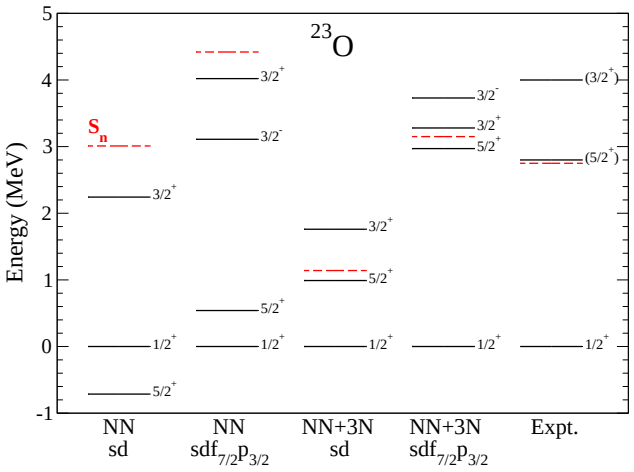

FIG. 17 Excitation energies of bound excited states in ^{23}O compared with experiment (Elekes *et al.* (2007); Schiller *et al.* (2007)). The NN-only results are calculated in the *sd* and $sdf_{7/2}p_{3/2}$ shells with empirical single-particle energies (SPEs). The NN+3N energies are obtained in the same spaces, but with calculated SPEs including 3NFs at N^{2}LO. For details see Holt *et al.* (2011). The dashed lines give the one-neutron separation energy S_n.

This oxygen anomaly is not reproduced in shell-model calculations derived from microscopic NN forces (see NN in Fig. 16 (b) and (c)), only with phenomenological adjustments (Fig. 16 (a)). As shown in Fig. 16 (c), chiral 3NFs at N^{2}LO lead to repulsive contributions to the interactions among excess neutrons that change the location of the neutron dripline from ^{28}O to the experimentally observed ^{24}O (Otsuka *et al.* (2009)). This is dominated by the long-range two-pion-exchange part of 3NFs, as demonstrated in Fig. 16 (b) and (c) with the single-Δ-excitation Fujita-Miyazawa 3NF (of the type of Fig. 1). For valence neutrons, the latter contribution is repulsive, which can be understood based on the Pauli principle (Otsuka *et al.* (2009)). This presents the first microscopic explanation of the oxygen anomaly. Since the 3NF mechanism is robust and general, these findings can impact the nucleosynthesis of heavy elements in neutron-rich environments. The same 3NF contributions have been shown to be key for the calcium isotopes (Gallant *et al.* (2012)) and for valence-proton interactions for proton-rich nuclei (Holt *et al.* (2012a)).

Occupying a position between two neutron-rich, doubly-magic isotopes, ^{22}O and ^{24}O, the spectrum of ^{23}O in Fig. 17 provides a unique test for theory, as it should reflect the features of both neighbors. In Fig. 17, we observe that 3NF contributions in extended valence spaces improve the spectrum considerably (Holt *et al.* (2011)). With NN forces, the first excited state is only at ≈ 0.5 MeV, well below experiment, similar to coupled-cluster theory with a N^{3}LO NN potential (Hagen *et al.* (2009)). Important future developments here are to include the continuum for loosely bound and unbound states (Michel *et al.* (2010)). Similar results for the oxygen and calcium isotopes have recently been obtained in coupled-cluster calculations including also the continuum, where 3NF effects are modeled through adjusted two-body interactions (Hagen *et al.* (2012a,b)).

Understanding and predicting the formation and evolution of shell structure from nuclear forces is another key challenge. While the magic numbers $N = 2, 8, 20$ are generally well understood, $N = 28$ is the first standard magic number that is not reproduced in microscopic theories with NN forces only (Caurier *et al.* (2005)). In a first study for calcium isotopes (Holt *et al.* (2012b)), it was shown that 3NFs are key to explain the $N = 28$ magic number, leading to a high 2^+ excitation energy and a concentrated magnetic dipole transition strength

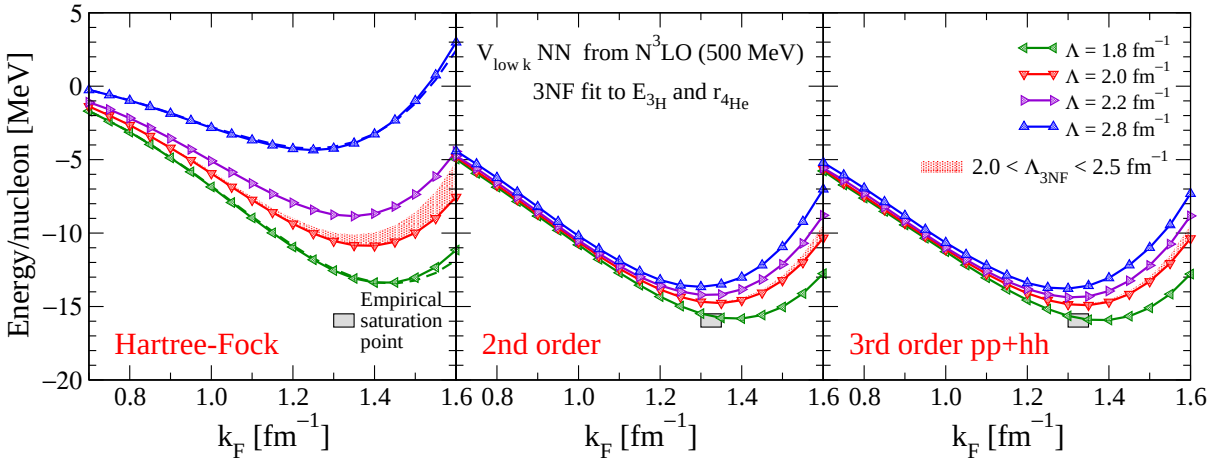

FIG. 18 (Color online) Nuclear matter energy per particle versus Fermi momentum k_F at the Hartree-Fock level (left) and including second-order (middle) and third-order particle-particle/hole-hole contributions (right), based on evolved N^{3}LO NN potentials and N^{2}LO 3NFs fit to the ^{3}H binding energy and the ^{4}He charge radius (Hebeler *et al.* (2011)). Theoretical uncertainties are estimated by the NN (lines)/3N (band) cutoff variations.

in ^{48}Ca (von Neumann-Cosel *et al.* (1998)).

The calculations of neutron-rich nuclei take into account the normal-ordered two-body part of 3NFs, which arises from the interactions of two valence neutrons with a nucleon in the core (see Fig. 16 (d)), which is enhanced by the number of core nucleons. Moreover, the normal-ordered two-body part can be shown to dominate over residual three-body interactions based on phase space arguments for normal Fermi systems (Friman and Schwenk (2011)). The normal-ordered two-body approximation has been demonstrated to be effective in coupled-cluster theory (Hagen *et al.* (2007)), with recent very promising results for medium-mass closed-shell nuclei (Roth *et al.* (2012)). In the context of the shell model, residual 3NFs were recently shown to be small, but amplified with neutron number in neutron-rich nuclei (Caesar *et al.* (2012)). In addition, normal-ordering techniques have been used to implement the SRG evolution of nuclear Hamiltonians directly "in-medium" in the A-body system of interest (Tsukiyama *et al.* (2011)).

Recent developments of chiral EFT and RG transformations for nuclear forces enable controlled calculations of matter at nuclear densities. Nuclear matter calculations provide an important benchmark for nuclear forces, and are used to constrain calculations of heavy nuclei and matter in astrophysics. The RG evolution to low momenta softens the short-range tensor components and short-range repulsion of nuclear forces (Bogner *et al.* (2006)). This leads to contributions in the particle-particle channel that are well converged at second order in the potential, suggesting that perturbative approaches can be used in place of the Bethe-Brueckner-Goldstone hole-line expansion (Bogner *et al.* (2005); Hebeler *et al.* (2011)). In this framework, it is also possible to estimate the theoretical uncertainties due to neglected many-body forces and from an incomplete many-body calculation. The nuclear matter results starting from chiral EFT interactions are shown in Fig. 18. Three-nucleon forces drive saturation, and these are the first nuclear forces fit only to $A \leqslant 4$ nuclei that predict realistic saturation properties. For these developments, an improved treatment of 3NFs as density-dependent two-body interactions has been key (Holt *et al.* (2010); Hebeler and Schwenk (2010)). The rapid convergence around saturation density in Fig. 18 may justify in part the application of in-medium chiral perturbation theory (Lutz *et al.* (2000); Kaiser *et al.* (2002); Lacour *et al.* (2011)), which provides an alternative expansion for nuclear densities. In in-medium chiral perturbation theory, the inclusion of long-range two-pion-exchange 3NFs from Δ degrees of freedom also improves the description of nuclear matter and the convergence (Fritsch *et al.* (2005)). In addition, 3NF contributions to the quasiparticle interactions in nuclear matter have been explored in Holt *et al.* (2012c).

The nuclear matter results imply that exchange correlations are tractable, which opens the door to develop a universal nuclear energy density functional (UNEDF) for global ground-state predictions based on microscopic interactions. This is one of the goals of the SciDAC UNEDF/NUCLEI initiatives. Three-nucleon forces play a key role in this, including for an improved density matrix expansion based on chiral EFT interactions (see, e.g., Stoitsov *et al.* (2010)) and for systematic studies of pairing in nuclei with a non-empirical pairing functional (Lesinski *et al.* (2012)).

For neutron matter, only the long-range two-pion-exchange c_1 and c_3 parts of N^{2}LO 3NFs contribute

TABLE III Symmetry energy $E_{\rm sym}$ obtained from neutron matter calculations with N^{2}LO 3NFs for different c_1 and c_3 couplings and based on RG-evolved N^{3}LO NN forces only (Hebeler *et al.* (2010)).

c_1 [GeV^{-1}]	c_3 [GeV^{-1}]	$E_{\rm sym}$ [MeV]
−0.7	−2.2	30.1
−1.4	−4.8	34.4
NN-only (Entem and Machleidt (2003))		26.5
NN-only (Epelbaum *et al.* (2005))		25.6

(Hebeler and Schwenk (2010); Tolos *et al.* (2008)). This has allowed for a detailed study of the theoretical uncertainties of the neutron matter energy (Hebeler and Schwenk (2010)). The inclusion of 3NFs leads to an energy per particle at saturation density $E_n(\rho_0)/N = 16.3 \pm 2.2\,\text{MeV}$, where the uncertainty is dominated by the uncertainty in the c_3 coupling (and to a smaller extent by c_1; see the c_1, c_3 range in Table I). Other microscopic calculations lie within this energy range. The uncertainty of the prediction is again an estimate of the importance of including N^{3}LO contributions for neutron and nuclear matter. Part of the N^{3}LO 4N forces has been estimated in neutron and nuclear matter (Fiorilla *et al.* (2012)), and a first complete N^{3}LO calculation of neutron matter including NN, 3N and 4N forces has recently been carried out (Tews *et al.* (2012)). The predicted neutron matter energy also provides constraints for the symmetry energy (see Table III, which demonstrates that the uncertainty in 3NFs dominates), and predicts the neutron skin thickness of ^{208}Pb to $0.17 \pm 0.03\,\text{fm}$, in excellent agreement with a recent determination from the complete electric dipole response (Tamii *et al.* (2011)). These developments are complemented by Auxiliary Field Diffusion Monte Carlo calculations using a range of phenomenological 3NFs (Gandolfi *et al.* (2012)) and by lattice simulations with chiral 3NFs of dilute neutron matter (Epelbaum *et al.* (2009b)), which can also enable future benchmarks at nuclear densities of the perturbative neutron matter calculations

These advances have an important impact on astrophysics. The microscopic calculations based on chiral EFT interactions constrain the properties of neutron-rich matter below nuclear densities to a much higher degree than is reflected in current neutron star modeling (Hebeler *et al.* (2010)). Combined with the heaviest $1.97 M_\odot$ neutron star (Demorest *et al.* (2010)), the neutron matter results based on chiral NN and 3N interactions constrain the radius of a typical $1.4 M_\odot$ star to $R \approx 10 - 14\,\text{km}$ ($\pm 15\%$), as shown in Fig. 19. The predicted radius range is due, in about equal amounts, to the uncertainty in 3N (and higher-body) forces and to the extrapolation to high densities. The predicted range is also

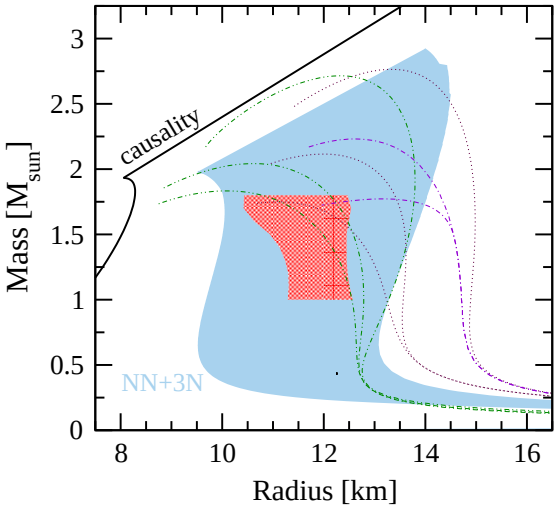

FIG. 19 (Color online) Mass-radius range for neutron stars based on chiral EFT NN+3N interactions, combined with a general extrapolation to high densities (Hebeler *et al.* (2010); the light blue/grey region includes an update for the 1.97 neutron star discovered recently). The predicted range is consistent with astrophysical modeling of X-ray burst sources (see, e.g., the red/gray shaded region from the Steiner *et al.* (2010) analysis). For comparison, we also show equations of state commonly used in supernova simulations (lines from O'Conner (2011)).

consistent with astrophysical results obtained from modeling X-ray burst sources (see, e.g., Steiner *et al.* (2010) in Fig. 19). In addition, the comparisons in Fig. 19 demonstrate that the constraints resulting from chiral EFT should be included in equations of state used for simulations of stellar collapse, black-hole formation, and neutron stars.

VI. THREE-BODY FORCES AND RELATIONS TO OTHER PROCESSES

Because of gauge symmetries, the same expansion is used to derive nuclear forces and electroweak operators. Therefore, the couplings of three-body forces in an EFT determine also electroweak processes. This is an important consistency test and makes such theories very predictive.

A prime example in chiral EFT are electroweak axial currents, where pion couplings contribute both to the currents and to nuclear forces. This is already seen at leading order: g_A determines the axial one-body current and the one-pion-exchange potential. Two-body currents, also known as meson-exchange currents, enter at higher order, just like 3NFs. As shown in Fig. 20, the leading axial contributions (at order Q^3) are due to long-range one-pion-exchange and short-range parts (Park *et al.* (2003)), with the same couplings c_3, c_4

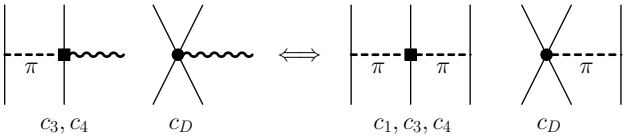

FIG. 20 Leading two-body axial currents and the corresponding 3NF contributions in chiral EFT. Solid (dashed) lines indicate nucleons (pions), and the wavy line represents the axial current.

and c_D of N^{2}LO 3NFs (Gårdestig and Phillips (2006); Gazit *et al.* (2009)). Chiral EFT is essential for this connection, which can be viewed as the two-body analogue of the Goldberger-Treiman relation.

Two-body currents have also been derived for electromagnetic reactions (Pastore *et al.* (2008); Kölling *et al.* (2009); Pastore *et al.* (2009); Pastore *et al.* (2011); Kölling *et al.* (2011)). Their application to the few-nucleon system has just started, but based on model interactions one can expect an interesting sensitivity of many electromagnetic reactions to two-body currents and 3NFs (Bacca *et al.* (2009); Golak *et al.* (2005)). In this colloquium, we focus on recent developments with electroweak axial currents beyond light nuclei.

Figure 20 demonstrates the unique constraints chiral EFT provides for two-body axial currents and 3NFs. This relates the interactions with external probes to the strong-interaction dynamics in nuclei. In particular, the low-energy coupling c_D that determines the mid-range one-pion-exchange 3NF can be determined either from the structure of light nuclei (see Section V); through the two-body axial currents that enter weak decays such as the ^{3}H half-life; or from pion production in hadronic collisions.[2] This consistency opens up new avenues of research for weak interactions and fundamental symmetries.

Although the importance of two-body currents is known from phenomenological studies, for weak processes, chiral currents and the consistency with nuclear forces have only been explored in light nuclei (Park *et al.* (2003); Gazit *et al.* (2009); Kubodera and Rho (2011)). Figure 21 shows the dependence of the ^{3}H half-life on the low-energy coupling c_D, which is included both in the leading 3NFs and two-body axial currents. Without 3NFs and without two-body currents, the experimental ^{3}H half-life is not reproduced. A dependence on the different N^{3}LO NN potentials is expected, because the leading 3NFs and two-body axial currents are

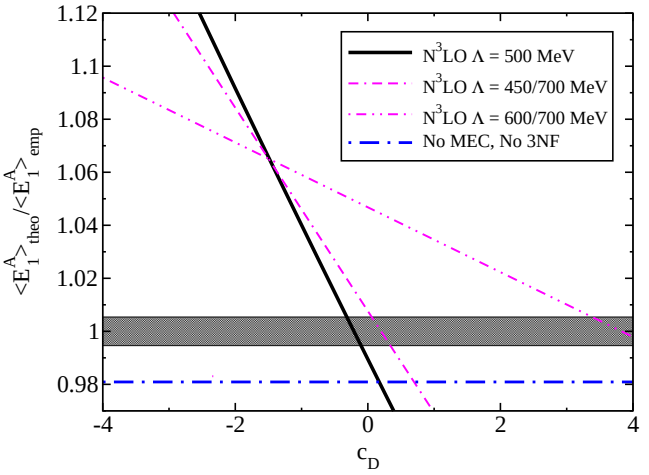

FIG. 21 (Color online) The ratio $\langle E_1^A\rangle_{\rm theo}/\langle E_1^A\rangle_{\rm emp}$ that determines the ^{3}H half-life as a function of the low-energy coupling c_D, which relates the leading two-body axial currents and 3NFs (see Fig. 20). The empirical range is given by the horizontal band. Results are shown based on different N^{3}LO NN potentials and including N^{2}LO 3NFs and consistent two-body axial currents. For comparison, the result without 3NFs and without two-body currents (No MEC, No 3NF) is given. For details see Gazit *et al.* (2009).

only order Q^3. As for 3NFs, the next order two-body axial currents are predicted in chiral EFT, without free parameters, which enables systematic improvements of beta-decay studies and predictions. The chiral EFT currents determined from the ^{3}H half-life have recently been applied to the beta decay of the two-neutron halo nucleus ^{6}He (Vaintraub *et al.* (2009)), however using a phenomenological potential model not based on chiral EFT, where the decay rate is satisfactorily reproduced. These theoretical studies are complemented by precision measurements (see the recent result for the ^{6}He half-life (Knecht *et al.* (2012))).

Surprisingly, key aspects of well-known beta decays in medium-mass nuclei remain a puzzle. In particular, when calculations of Gamow-Teller (GT) transitions of the spin-isospin operator $g_A\boldsymbol{\sigma}\tau^{\pm}$ are confronted with experiment (this is the most significant operator for beta decays and for electron-capture processes), some degree of renormalization, or "quenching" q, of the axial coupling $g_A^{\rm eff} = qg_A$ is needed. Compared to the single-nucleon value $g_A = 1.2695(29)$, the GT term seems to be weaker in nuclei. This was first conjectured in studies of beta-decay rates, with a typical $q \approx 0.75$ in shell-model calculations (Wildenthal *et al.* (1983); Martinez-Pinedo *et al.* (1996)) and other many-body approaches (Bender *et al.* (2002); Rodriguez and Martinez-Pinedo (2010)). In view of the significant effect on weak reaction rates, it is no surprise that this suppression has been the target of many theoretical works (see the discussion in Vaintraub *et al.* (2009)).

[2] The low-energy coupling c_D also enters pion production in NN collisions. However, this probes significantly higher momenta, because of the produced pion. For nuclear forces, the determination in pion production may therefore not be as effective as from the low-momentum kinematics involved in nuclear structure (Pandharipande *et al.* (2005)).

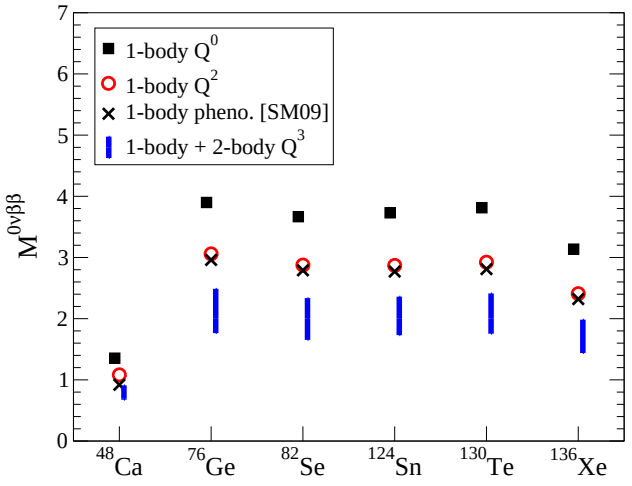

FIG. 22 (Color online) Nuclear matrix elements $M^{0\nu\beta\beta}$ for neutrino-less double-beta decay of different nuclei. Results are shown based on chiral EFT currents at successive orders, including one-body currents at orders Q^0 and Q^2, and the predicted long-range parts of two-body currents at order Q^3 (Menendez *et al.* (2011); for a discussion of the short-range contributions, see this reference). For comparison, we also show shell-model results (SM09) of Menendez *et al.* (2009) based on phenomenological one-body currents only.

Recent studies of GT transitions in medium-mass nuclei with chiral EFT currents provide new insights and opportunities to this puzzle (Menendez *et al.* (2011)). Compared to light nuclei, the contributions of chiral two-body currents are amplified in medium-mass nuclei because of the larger nucleon momenta. Using a normal-ordering approximation for two-body currents to create a density-dependent operator, it was shown that the leading two-body axial currents contribute only to the GT operator (up to a small tensor-like correction) and that a quenching of low-momentum-transfer GT transitions is predicted based on the long-range parts of two-body currents. This demonstrates that chiral two-body currents naturally contribute to the quenching of GT transitions. A reduction of g_A in the currents is also expected considering chiral 3NFs as density-dependent two-body interactions (Holt *et al.* (2009, 2010)). The long-range one-body contributions from two-body currents are in part due to Delta-hole pairs, but it remains an open problem how much of the quenching of g_A is due to two-body currents and how much due to polarization effects.

Neutrinoless double-beta decay presents a fundamental test of the nature of the neutrino, of lepton number, and the neutrino mass scale and hierarchy (Elliott and Vogel (2002); Avignone III *et al.* (2008)). A pivotal input for the ongoing and planned experimental searches are the nuclear matrix elements that incorporate the structure of the parent and daughter nuclei and of the decay mechanism. Compared to standard beta decays, neutrinoless double-beta decay probes different momentum transfers $Q \approx 100\,\mathrm{MeV} \sim m_\pi$ (Simkovic *et al.* (2008); Menendez *et al.* (2011)). Therefore, the impact of two-body currents is unclear and renormalization effects can differ from the suppression of g_A in medium-mass nuclei. Chiral EFT predicts the momentum-transfer dependence of two-body currents, which varies on the order of the pion mass due to the one-pion-exchange part in Fig. 20. The first calculation of the neutrinoless double-beta decay operator based on chiral EFT currents at successive order is shown in Fig. 22. This demonstrates that the contributions from two-body currents are significant and should be included in all calculations. It also shows how chiral EFT can provide key input and theoretical uncertainties for fundamental symmetry tests with nuclei. Recently, chiral EFT currents have also been applied to calculate the structure factor for spin-dependent weakly interacting massive particle (WIMP) scattering off nuclei, needed for direct dark matter detection (Menéndez *et al.* (2012)).

VII. OUTLOOK AND FUTURE OPPORTUNITIES

In this colloquium, we have highlighted the importance of three-body forces in nuclear physics and related areas. Here, we give an outlook with a focus on future opportunities and challenges. Our discussion is guided by Fig. 23 which summarizes the leading 3NFs in different EFTs and shows the order in the expansion at which they enter.

In pionless EFT for systems with large two-body scattering lengths discussed in Section III, three-body forces contribute already at leading order because of the Efimov effect. If observables are considered at fixed scattering lengths, subleading three-body forces are suppressed by two orders and enter only at N^{2}LO. Some higher-order calculations of few-nucleon observables exist but much remains to be investigated in this sector. Particularly interesting are the application of pionless EFT to halo nuclei and low-energy electroweak reactions. Halo nuclei are the most promising candidates for observing Efimov physics in nuclei, while precise calculations of low-energy reactions are relevant for nuclear astrophysics and neutrino physics. In particular, 3NFs play a prominent role in two-neutron halo nuclei and larger halo systems. Pionless EFT also predicts universal three-body correlations that can be explored in nuclear reactions in this regime and to test the consistency of different theoretical calculations (similar to the Tjon line/band).

In chiral EFT discussed in Sections IV, V and VI, 3NFs are suppressed compared to NN interactions. This explains the phenomenological success of weaker three-body forces of the Fujita-Miyazawa type. As summarized in Fig. 23, 3NFs enter at N^{2}LO, and their relative contributions to observables can be understood based on the

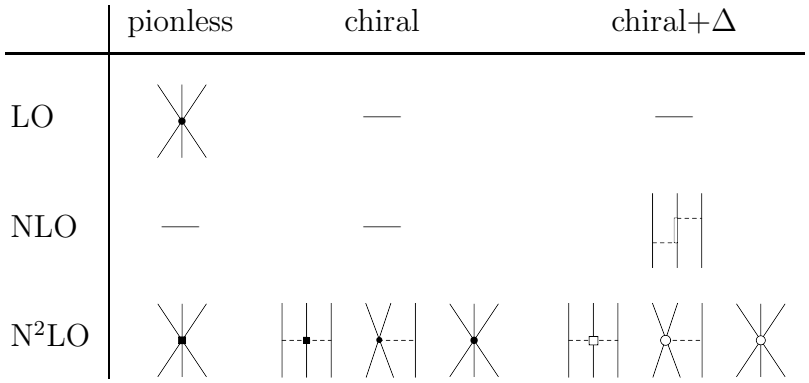

FIG. 23 Order of 3NF contributions in pionless and chiral EFT and in EFT with explicit Δ degrees of freedom (chiral+Δ). Open vertices in the last column indicate the differences of the low-energy constants in chiral and chiral+Δ EFT.

power counting. Because the operator structure of the leading 3NFs is strongly constrained, a global analysis of few-body scattering and bound-state data with theoretical uncertainties appears feasible in the framework of chiral EFT. This would allow for a determination of the long-range c_i couplings in the three-body sector. In addition, a consistent determination of two- and three-body forces from such an analysis may help to resolve the A_y puzzle in few-body scattering.

For applications of chiral EFT interactions to nuclear structure, 3NFs play a central role, as discussed for light and medium-mass nuclei and for nuclear matter. For these many-body calculations, the RG evolution leads to greatly improved convergence. A consistent evolution of chiral 3NFs has been achieved in a harmonic-oscillator basis and recently in momentum space. Important open problems are an understanding of the 3NFs induced by the SRG and to control higher-body forces, which is necessary for the desired accuracy in nuclear structure.

If $\Delta(1232)$ degrees of freedom are included, part of the physics contained in the low-energy constants in chiral EFT is made explicit in lower orders. As a consequence, a 3NF of the Fujita-Miyazawa type appears already at NLO as shown in Fig. 23. Improved convergence of the chiral expansion with explicit Δ degrees of freedom is expected, but a full analysis of few-nucleon data remains to be carried out. In addition, a chiral EFT with explicit Δ's would naturally explain why the contributions from the long-range two-pion-exchange parts of 3NFs dominate over the shorter-range parts in applications to neutron-rich nuclei and nuclear matter.

Three-nucleon forces are a frontier in the physics of nuclei that connects the systematic development of nuclear forces in chiral EFT with the exploration of neutron-rich nuclei at rare isotope beam facilities. The subleading 3NFs at N^{3}LO are predicted in chiral EFT, without free parameters, as is the case for N^{3}LO 4N forces. In many present calculations, the uncertainty of the leading 3NFs likely dominates the theoretical uncertainties of the predicted observables. The derivation of N^{3}LO 3NFs has only been completed recently, and no calculation exists with N^{3}LO 3N or 4N forces beyond few-body systems. Therefore, there is a window of opportunity to make key discoveries and predictions. In addition to advancing microscopic calculations with 3NFs to larger and neutron-rich nuclei, an important problem is to understand the impact of 3NFs on global nuclear structure predictions, e.g., for key regions in the r-process path where systematic theoretical predictions of extreme nuclei, often not accessible in the laboratory, are needed.

Electroweak interaction processes are unique probes of the physics of nuclei and fundamental symmetries, and play a central role in astrophysics. Chiral EFT provides a systematic basis for nuclear forces and consistent electroweak currents, where pion couplings contribute both to electroweak currents and to 3NFs. This opens up new opportunities for precise nuclear structure calculations with theoretical uncertainties that are needed for fundamental symmetry tests with beta decays and weak transitions, including the key nuclear matrix elements for neutrinoless double-beta decay.

In principle, it is possible to calculate nuclear properties directly from the QCD Lagrangian. In Lattice QCD, the QCD path integral is evaluated in a discretized Euclidean space-time using Monte Carlo simulations. This approach is based on a nonperturbative formulation of QCD but requires a large numerical effort. However, high statistics Lattice QCD simulations of two- and three-nucleon systems are now within reach (Beane *et al.* (2011)) and the calculation of few-nucleon systems appears feasible in the intermediate future. A milestone for nuclear forces is the prediction of three-neutron properties in a box. This will provide unique access to the isospin $T = 3/2$ component of 3NFs, which is not probed in nucleon-deuteron scattering. Moreover, Lattice QCD results can also be used to constrain couplings in chiral 3NFs. A first step in this direction was recently carried out by Doi *et al.* (2012).

ACKNOWLEDGMENTS

We thank R. J. Furnstahl, U.-G. Meißner, D. R. Phillips and W. Weise for comments on the manuscript. Many discussions with our collaborators on the topics of this colloquium are gratefully acknowledged. This work was supported by the DFG through SFB/TR 16 and SFB 634, by the BMBF under contracts No. 06BN9006 and No. 06DA70471, by the JSC, Jülich, by the Helmholtz Alliance Program of the Helmholtz Association, contract HA216/EMMI "Extremes of Density and Temperature: Cosmic Matter in the Laboratory", and by the ERC grant No. 307986 STRONGINT.

REFERENCES

Afnan, I. R., and F. J. D. Serduke, 1973, Phys. Lett. **B44**, 143 .
Amghar, A., and B. Desplanques, 1995, Nucl. Phys. **A585**, 657.
Avignone III, F. T., S. R. Elliott, and J. Engel, 2008, Rev. Mod. Phys. **80**, 481.
Bacca, S., N. Barnea, W. Leidemann, and G. Orlandini, 2009, Phys. Rev. Lett. **102**, 162501.
Beane, S. R., P. F. Bedaque, W. C. Haxton, D. R. Phillips, and M. J. Savage, 2001, in *At the Frontier of Particle Physics: Handbook of QCD*, edited by M. Shifman and B. L. Ioffe (World Scientific), eprint nucl-th/0008064.
Beane, S. R., W. Detmold, K. Orginos, and M. J. Savage, 2011, Prog. Part. Nucl. Phys. **66**, 1.
Bedaque, P. F., H.-W. Hammer, and U. van Kolck, 1998, Phys. Rev. **C 58**, 641.
Bedaque, P. F., H.-W. Hammer, and U. van Kolck, 1999a, Phys. Rev. Lett. **82**, 463.
Bedaque, P. F., H.-W. Hammer, and U. van Kolck, 1999b, Nucl. Phys. **A646**, 444.
Bedaque, P. F., H.-W. Hammer, and U. van Kolck, 2003a, Phys. Lett. **B569**, 159.
Bedaque, P. F., and U. van Kolck, 1998, Phys. Lett. **B428**, 221.
Bedaque, P. F., and U. van Kolck, 2002, Ann. Rev. Nucl. Part. Sci. **52**, 339.
Bedaque, P. F., G. Rupak, H. W. Grießhammer, and H.-W. Hammer, 2003b, Nucl. Phys. **A714**, 589.
Bender, M., J. Dobaczewski, J. Engel, and W. Nazarewicz, 2002, Phys. Rev. **C 65**, 054322.
Bernard, V., E. Epelbaum, H. Krebs, and U.-G. Meißner, 2008, Phys. Rev. **C 77**, 064004.
Bernard, V., E. Epelbaum, H. Krebs, and U.-G. Meißner, 2011, Phys. Rev. **C 84**, 054001.
Bernard, V., N. Kaiser, and U.-G. Meißner, 1997, Nucl. Phys. **A615**, 483.
Bertsch, G. F., 1999, Many-Body-Theory Challenge Problem posed for the Conference on Recent Progress in Many-Body Theories, see also Preface of the Proceedings in IJMP B **15** Nos. 10-11 (2001).
Bertulani, C. A., H. W. Hammer, and U. Van Kolck, 2002, Nucl. Phys. **A712**, 37.
Beth, E., and G. Uhlenbeck, 1937, Physica **4**, 915.
Bogner, S. K., R. J. Furnstahl, and R. J. Perry, 2007a, Phys. Rev. **C 75**, 061001.
Bogner, S. K., R. J. Furnstahl, S. Ramanan, and A. Schwenk, 2006, Nucl. Phys. **A773**, 203.
Bogner, S. K., R. J. Furnstahl, S. Ramanan, and A. Schwenk, 2007b, Nucl. Phys. **A784**, 79.
Bogner, S. K., R. J. Furnstahl, and A. Schwenk, 2010, Prog. Part. Nucl. Phys. **65**, 94.
Bogner, S. K., T. T. S. Kuo, and A. Schwenk, 2003, Phys. Rept. **386**, 1.
Bogner, S. K., A. Schwenk, R. J. Furnstahl, and A. Nogga, 2005, Nucl. Phys. **A763**, 59.
Braaten, E., and H.-W. Hammer, 2003, Phys. Rev. Lett. **91**, 102002.
Braaten, E., and H.-W. Hammer, 2006, Phys. Rept. **428**, 259.
Brodeur, M., T. Brunner, C. Champagne, S. Ettenauer, M. Smith, A. Lapierre, R. Ringle, V. L. Ryjkov, S. Bacca, P. Delheij, G. W. F. Drake, D. Lunney, *et al.*, 2012, Phys. Rev. Lett. **108**, 052504.
Büttiker, P., and U.-G. Meißner, 2000, Nucl. Phys. **A668**, 97.
Caesar, C., *et al.*, 2012, eprint 1209.0156.
Caurier, E., G. Martinez-Pinedo, F. Nowacki, A. Poves, and A. Zuker, 2005, Rev. Mod. Phys. **77**, 427.
Coester, F., S. Cohen, B. Day, and C. M. Vincent, 1970, Phys. Rev. **C 1**, 769.
Coleman, S. R., J. Wess, and B. Zumino, 1969, Phys. Rev. **177**, 2239.
Coon, S. A., M. D. Scadron, P. C. McNamee, B. R. Barrett, D. W. E. Blatt, and B. H. J. McKellar, 1979, Nucl. Phys. **A317**, 242.
Danilov, G., 1961, Sov. Phys. JETP **13**, 349.
Deltuva, A., 2012, Phys. Rev. **A 85**, 012708.
Deltuva, A., A. C. Fonseca, and P. U. Sauer, 2008, Phys. Lett. **B660**, 471.
Demorest, P. B., T. Pennucci, S. M. Ransom, M. S. E. Roberts, and J. W. T. Hessels, 2010, Nature **467**, 1081.
Doi, T., S. Aoki, T. Hatsuda, Y. Ikeda, T. Inoue, N. Ishii, K. Murano, H. Nemura, and K. Sasaki (HAL QCD Collaboration), 2012, Prog. Theor. Phys. **127**, 723.
Efimov, V., 1970, Phys. Lett. **B33**, 563.
Elekes, Z., Z. Dombrádi, N. Aoi, S. Bishop, Z. Fülöp, J. Gibelin, T. Gomi, Y. Hashimoto, N. Imai, N. Iwasa, H. Iwasaki, G. Kalinka, *et al.*, 2007, Phys. Rev. Lett. **98**, 102502.
Elliott, S. R., and P. Vogel, 2002, Ann. Rev. Nucl. Part. Sci. **52**, 115.
Entem, D. R., and R. Machleidt, 2002, Phys. Rev. **C 66**, 014002.
Entem, D. R., and R. Machleidt, 2003, Phys. Rev. **C 68**, 041001.
Epelbaum, E., 2006, Prog. Part. Nucl. Phys. **57**, 654.
Epelbaum, E., 2007, Eur. Phys. J. **A 34**, 197.
Epelbaum, E., and J. Gegelia, 2009, Eur. Phys. J. **A 41**, 341.
Epelbaum, E., W. Glöckle, and U.-G. Meißner, 2005, Nucl. Phys. **A747**, 362.
Epelbaum, E., H.-W. Hammer, and U.-G. Meißner, 2009a, Rev. Mod. Phys. **81**, 1773.
Epelbaum, E., H. Krebs, D. Lee, and U.-G. Meißner, 2009b, Eur. Phys. J. **A 41**, 125.
Epelbaum, E., H. Krebs, D. Lee, and U.-G. Meißner, 2011, Phys. Rev. Lett. **106**, 192501.
Epelbaum, E., H. Krebs, and U.-G. Meißner, 2008, Nucl. Phys. **A806**, 65.
Epelbaum, E., A. Nogga, W. Glöckle, H. Kamada, U.-G. Meißner, and H. Witała, 2002, Phys. Rev. **C 66**, 064001.
Ferlaino, F., and R. Grimm, 2010, Physics **3**, 9.

Ferlaino, F., S. Knoop, M. Berninger, W. Harm, J. P. D'Incao, H.-C. Nägerl, and R. Grimm, 2009, Phys. Rev. Lett. **102**, 140401.

Fernando, L., R. Higa, and G. Rupak, 2011, eprint 1109.1876.

Fettes, N., U.-G. Meißner, and S. Steininger, 1998, Nucl. Phys. **A640**, 199.

Fiorilla, S., N. Kaiser, and W. Weise, 2012, Nucl.Phys. **A880**, 65.

Friar, J. L., D. Hüber, and U. van Kolck, 1999, Phys. Rev. **C 59**, 53.

Friman, B., and A. Schwenk, 2011, in *From Nuclei to Stars: Festschrift in Honor of Gerald E. Brown*, edited by S. Lee (World Scientific), p. 141, eprint 1101.4858.

Fritsch, S., N. Kaiser, and W. Weise, 2005, Nucl. Phys. **A750**, 259.

Fujita, J., and H. Miyazawa, 1957, Prog. Theor. Phys. **17**, 360.

Furnstahl, R. J., H. W. Hammer, and N. Tirfessa, 2001, Nucl. Phys. **A689**, 846.

Gallant, A. T., *et al.*, 2012, Phys. Rev. Lett. **109**, 032506.

Gandolfi, S., J. Carlson, and S. Reddy, 2012, Phys. Rev. **C 85**, 032801.

Gårdestig, A., and D. R. Phillips, 2006, Phys. Rev. Lett. **96**, 232301.

Gazit, D., S. Quaglioni, and P. Navrátil, 2009, Phys. Rev. Lett. **103**, 102502.

Giorgini, S., L. P. Pitaevskii, and S. Stringari, 2008, Rev. Mod. Phys. **80**, 1215.

Golak, J., R. Skibiński, H. Witała, W. Glöckle, A. Nogga, and H. Kamada, 2005, Phys. Rept. **415**, 89.

Grießhammer, H. W., 2005, Nucl. Phys. **A760**, 110.

Gross, N., Z. Shotan, S. Kokkelmans, and L. Khaykovich, 2010, Phys. Rev. Lett. **105**, 103203.

Haag, R., 1958, Phys. Rev. **112**, 669.

Hadizadeh, M., M. Yamashita, L. Tomio, A. Delfino, and T. Frederico, 2011, Phys. Rev. Lett. **107**, 135304.

Hagen, G., M. Hjorth-Jensen, G. R. Jansen, R. Machleidt, and T. Papenbrock, 2012a, Phys. Rev. Lett. **108**, 242501.

Hagen, G., M. Hjorth-Jensen, G. R. Jansen, R. Machleidt, and T. Papenbrock, 2012b, Phys. Rev. Lett. **109**, 032502.

Hagen, G., T. Papenbrock, D. J. Dean, M. Hjorth-Jensen, and B. Velamur Asokan, 2009, Phys. Rev. **C 80**, 021306.

Hagen, G., T. Papenbrock, D. J. Dean, A. Schwenk, A. Nogga, M. Włoch, and P. Piecuch, 2007, Phys. Rev. **C 76**, 034302.

Hammer, H.-W., and R. J. Furnstahl, 2000, Nucl. Phys. **A678**, 277.

Hammer, H.-W., N. Kalantar-Nayestanaki, and D. R. Phillips, 2007, in *Chiral dynamics 2006: Proceedings of the 5th International Conference on Chiral Dynamics, Theory and Experiment*, edited by M. W. Ahmed, H. Gao, B. Holstein, and H. R. Weller (World Scientific), pp. 315–329, eprint nucl-th/0611084.

Hammer, H.-W., and D. Phillips, 2011, Nucl. Phys. **A865**, 17.

Hammer, H.-W., and L. Platter, 2007, Eur. Phys. J. **A 32**, 113.

Hammer, H.-W., and L. Platter, 2010, Ann. Rev. Nucl. Part. Sci. **60**, 207.

Hanna, G. J., and D. Blume, 2006, Phys. Rev. A **74**, 063604.

Hebeler, K., 2012, Phys. Rev. **C 85**, 021002.

Hebeler, K., S. K. Bogner, R. J. Furnstahl, A. Nogga, and A. Schwenk, 2011, Phys. Rev. **C 83**, 031301.

Hebeler, K., J. M. Lattimer, C. J. Pethick, and A. Schwenk, 2010, Phys. Rev. Lett. **105**, 161102.

Hebeler, K., and A. Schwenk, 2010, Phys. Rev. **C 82**, 014314.

Holt, J. D., J. Menendez, and A. Schwenk, 2011, eprint 1108.2680.

Holt, J. D., J. Menéndez, and A. Schwenk, 2012a, eprint 1207.1509.

Holt, J. D., T. Otsuka, A. Schwenk, and T. Suzuki, 2012b, J. Phys. **G 39**, 085111.

Holt, J. W., N. Kaiser, and W. Weise, 2009, Phys. Rev. **C 79**, 054331.

Holt, J. W., N. Kaiser, and W. Weise, 2010, Phys. Rev. **C 81**, 024002.

Holt, J. W., N. Kaiser, and W. Weise, 2012c, Nucl. Phys. **A876**, 61.

Howell, C. R., W. Tornow, K. Murphy, H. G. Pfützner, M. L. Roberts, A. Li, P. D. Felsher, R. L. Walter, I. Šlaus, P. A. Treado, and Y. Koike, 1987, Few Body Syst. **2**, 19.

Janssens, R. V. F., 2009, Nature **459**, 1069.

Ji, C., D. R. Phillips, and L. Platter, 2012, Annals Phys. **327**, 1803.

Jurgenson, E., P. Navrátil, and R. Furnstahl, 2011, Phys. Rev. **C 83**, 034301.

Jurgenson, E. D., S. K. Bogner, R. J. Furnstahl, and R. J. Perry, 2008, Phys. Rev. **C 78**, 014003.

Jurgenson, E. D., P. Navrátil, and R. J. Furnstahl, 2009, Phys. Rev. Lett. **103**, 082501.

Kaiser, N., S. Fritsch, and W. Weise, 2002, Nucl. Phys. **A697**, 255.

Kaiser, N., S. Gerstendorfer, and W. Weise, 1998, Nucl. Phys. **A637**, 395.

Kalantar-Nayestanaki, N., E. Epelbaum, J. G. Messchendorp, and A. Nogga, 2012, Rept. Prog. Phys. **75**, 016301.

Kaplan, D. B., M. J. Savage, and M. B. Wise, 1998, Nucl. Phys. **B534**, 329.

Kaplan, I. G., and O. Novaro, 1994, Revista Mexicana de Física **40**, 108.

Kirscher, J., H. W. Grießhammer, D. Shukla, and H. M. Hofmann, 2010, Eur. Phys. J. **A44**, 239.

Knecht, A., R. Hong, D. Zumwalt, B. Delbridge, A. Garcia, P. Mueller, H. E. Swanson, I. S. Towner, S. Utsuno, W. Williams, and C. Wrede, 2012, Phys. Rev. Lett. **108**, 122502.

van Kolck, U., 1994, Phys. Rev. **C 49**, 2932.

van Kolck, U., 1999, Nucl. Phys. **A645**, 273.

Kölling, S., E. Epelbaum, H. Krebs, and U.-G. Meißner, 2009, Phys. Rev. **C 80**, 045502.

Kölling, S., E. Epelbaum, H. Krebs, and U.-G. Meißner, 2011, Phys. Rev. **C 84**, 054008.

Krebs, H., E. Epelbaum, and U.-G. Meißner, 2007, Eur. Phys. J. **A 32**, 127.

Kubodera, K., and M. Rho, 2011, in *From Nuclei to Stars: Festschrift in Honor of Gerald E. Brown*, edited by S. Lee (World Scientific), p. 223, eprint 1011.4919.

Lacour, A., J. A. Oller, and U.-G. Meißner, 2011, Annals Phys. **326**, 241.

Lesinski, T., K. Hebeler, T. Duguet, and A. Schwenk, 2012, J. Phys. **G 39**, 015108.

Ley, J., C. D. Düweke, R. Emmerich, A. Imig, H. Paetz gen. Schieck, J. Golak, H. Witała, E. Epelbaum, A. Deltuva, A. C. Fonseca, W. Glöckle, U.-G. Meißner, *et al.*, 2006, Phys. Rev. **C 73**, 064001.

Lompe, T., T. B. Ottenstein, F. Serwane, A. N. Wenz, G. Zürn, and S. Jochim, 2010, Science **330**, 940.

Lutz, M. F., B. Friman, and C. Appel, 2000, Phys. Lett. **B474**, 7.

Machleidt, R., and D. R. Entem, 2011, Phys. Rept. **503**, 1.
Maris, P., J. P. Vary, P. Navrátil, W. E. Ormand, H. Nam, and D. J. Dean, 2011, Phys. Rev. Lett. **106**, 202502.
Martinez-Pinedo, G., A. Poves, E. Caurier, and A. Zuker, 1996, Phys. Rev. **C 53**, 2602.
Meißner, U.-G., 2007, On the low-energy constants of the chiral effective pion-nucleon Lagrangian, talk at the workshop on "Three-Nucleon Interactions from Few- to Many-Body Systems", TRIUMF, Vancouver, Canada.
Menendez, J., D. Gazit, and A. Schwenk, 2011, Phys. Rev. Lett. **107**, 062501.
Menéndez, J., D. Gazit, and A. Schwenk, 2012, eprint 1208.1094.
Menendez, J., A. Poves, E. Caurier, and F. Nowacki, 2009, Nucl. Phys. **A818**, 139.
Michel, N., W. Nazarewicz, J. Okolowicz, and M. Ploszajczak, 2010, J. Phys. **G 37**, 064042.
Miller, G. A., and A. Schwenk, 2007, Phys. Rev. **C 76**, 024001.
Mohr, R. F., R. J. Furnstahl, R. J. Perry, K. G. Wilson, and H. W. Hammer, 2006, Annals Phys. **321**, 225.
Nakajima, S., M. Horikoshi, T. Mukaiyama, P. Naidon, and M. Ueda, 2011, Phys. Rev. Lett. **106**, 143201.
Navrátil, P., V. G. Gueorguiev, J. P. Vary, W. E. Ormand, and A. Nogga, 2007, Phys. Rev. Lett. **99**, 042501.
von Neumann-Cosel, P., A. Poves, J. Retamosa, and A. Richter, 1998, Phys. Lett. **B443**, 1.
Newton, I., 1687, *Philosophiae Naturalis Principia Mathematica* (Joseph Streater, London).
Nogga, A., S. K. Bogner, and A. Schwenk, 2004, Phys. Rev. **C 70**, 061002.
Nogga, A., E. Epelbaum, J. Golak, H. Kamada, H. Witała, D. Rozpędzik, R. Skibiński, and W. Glöckle, 2010, in *19th International IUPAP Conference on Few-Body Problems in Physics*, volume 3 of *EPJ Web of Conferences*, p. 05006, August 31 - September 5, 2009.
Nogga, A., H. Kamada, and W. Glöckle, 2000, Phys. Rev. Lett. **85**, 944.
Nogga, A., P. Navrátil, B. R. Barrett, and J. P. Vary, 2006, Phys. Rev. **C 73**, 064002.
Nogga, A., R. G. E. Timmermans, and U. van Kolck, 2005, Phys. Rev. **C 72**, 054006.
Nollett, K. M., S. C. Pieper, R. B. Wiringa, J. Carlson, and G. M. Hale, 2007, Phys. Rev. Lett. **99**, 022502.
Nowacki, F., 2008, Cross-shell excitations in semi-magic nuclei, talk at conference on "From Quarks to the Nuclear Many-Body Problem", University of Oslo, Oslo, Norway.
O'Conner, E., 2011, private communication.
Ordóñez, C., L. Ray, and U. van Kolck, 1994, Phys. Rev. Lett. **72**, 1982.
Otsuka, T., T. Suzuki, J. D. Holt, A. Schwenk, and Y. Akaishi, 2009, Phys. Rev. Lett. **105**, 032501.
Pandharipande, V. R., D. R. Phillips, and U. van Kolck, 2005, Phys. Rev. **C 71**, 064002.
Park, T. S., L. E. Marcucci, R. Schiavilla, M. Viviani, A. Kievsky, S. Rosati, K. Kubodera, D.-P. Min, and M. Rho, 2003, Phys. Rev. **C 67**, 055206.
Pastore, S., L. Girlanda, R. Schiavilla, and M. Viviani, 2011, Phys. Rev. **C 84**, 024001.
Pastore, S., L. Girlanda, R. Schiavilla, M. Viviani, and R. B. Wiringa, 2009, Phys. Rev. **C 80**, 034004.
Pastore, S., R. Schiavilla, and J. L. Goity, 2008, Phys. Rev. **C 78**, 064002.
Phillips, A. C., 1968, Nucl. Phys. **A107**, 209.
Pieper, S. C., 2008, Riv. Nuovo Cim. **31**, 709.
Pieper, S. C., and R. B. Wiringa, 2001, Ann. Rev. Nucl. Part. Sci. **51**, 53.
Platter, L., 2009, Few Body Syst. **46**, 139.
Platter, L., H. W. Hammer, and U.-G. Meißner, 2004, Phys. Rev. **A 70**, 052101.
Platter, L., H. W. Hammer, and U.-G. Meißner, 2005, Phys. Lett. **B607**, 254.
Polyzou, W. N., and W. Glöckle, 1990, Few Body Syst. **9**, 97.
Rauprich, G., H. Hähn, M. Karus, P. Nießen, K. Nyga, H. Oswald, L. Sydow, H. Schieck, and Y. Koike, 1988, Few Body Syst. **5**, 67.
Rentmeester, M. C. M., R. G. E. Timmermans, and J. J. de Swart, 2003, Phys. Rev. **C 67**, 044001.
Rodriguez, T. R., and G. Martinez-Pinedo, 2010, Phys. Rev. Lett. **105**, 252503.
Roth, R., S. Binder, K. Vobig, A. Calci, J. Langhammer, *et al.*, 2012, Phys. Rev. Lett. **109**, 052501.
Roth, R., J. Langhammer, A. Calci, S. Binder, and P. Navrátil, 2011, Phys. Rev. Lett. **107**, 072501.
Rupak, G., and R. Higa, 2011, Phys. Rev. Lett. **106**, 222501.
Sagara, K., H. Oguri, S. Shimizu, Y. Maeda, H. Nakamura, T. Nakashima, and S. Morinobu, 1994, Phys. Rev. **C 50**, 576.
Schäfer, T., and D. Teaney, 2009, Rept. Prog. Phys. **72**, 126001.
Schiller, A., N. Frank, T. Baumann, D. Bazin, B. A. Brown, J. Brown, P. A. DeYoung, J. E. Finck, A. Gade, J. Hinnefeld, R. Howes, J.-L. Lecouey, *et al.*, 2007, Phys. Rev. Lett. **99**, 112501.
Simkovic, F., A. Faessler, V. Rodin, P. Vogel, and J. Engel, 2008, Phys. Rev. **C 77**, 045503.
Skorniakov, G. V., and K. A. Ter-Martirosian, 1957, Sov. Phys. JETP **4**, 648.
Sperisen, F., W. Grüebler, V. König, P. A. Schmelzbach, K. Elsener, B. Jenny, C. Schweizer, J. Ulbricht, and P. Doleschall, 1984, Nucl. Phys. **A422**, 81 .
von Stecher, J., 2010, J. Phys. B **43**, 101002.
von Stecher, J., 2011, Phys. Rev. Lett. **107**, 200402.
von Stecher, J., J. D'Incao, and C. Greene, 2009, Nature Physics **5**, 417.
Steiner, A. W., J. M. Lattimer, and E. F. Brown, 2010, Astrophys. J. **722**, 33.
Stoitsov, M., M. Kortelainen, S. Bogner, T. Duguet, R. Furnstahl, B. Gebremariam, and N. Schunck, 2010, Phys. Rev. **C 82**, 054307.
Tamii, A., I. Poltoratska, P. von Neumann-Cosel, Y. Fujita, T. Adachi, C. A. Bertulani, J. Carter, M. Dozono, H. Fujita, K. Fujita, K. Hatanaka, D. Ishikawa, *et al.*, 2011, Phys. Rev. Lett. **107**, 062502.
Tews, I., T. Krüger, K. Hebeler, and A. Schwenk, 2012, eprint 1206.0025.
Thomas, L. H., 1935, Phys. Rev. **47**, 903.
Tjon, J. A., 1975, Phys. Lett. **B56**, 217 .
Tolos, L., B. Friman, and A. Schwenk, 2008, Nucl. Phys. **A806**, 105.
Tsukiyama, K., S. Bogner, and A. Schwenk, 2011, Phys. Rev. Lett. **106**, 222502.
Vaintraub, S., N. Barnea, and D. Gazit, 2009, Phys. Rev. **C 79**, 065501.
Valderrama, M. P., 2011, Phys. Rev. **C 83**, 024003.
Viviani, M., L. Girlanda, A. Kievsky, L. E. Marcucci, and S. Rosati, 2010, in *19th International IUPAP Conference on Few-Body Problems in Physics*, volume 3 of *EPJ Web*

of Conferences, p. 05011, August 31 - September 5, 2009, eprint 1004.1306.

Viviani, M., A. Kievsky, S. Rosati, E. A. George, and L. D. Knutson, 2001, Phys. Rev. Lett. **86**, 3739.

Wang, Y., J. P. D'Incao, and C. H. Greene, 2011, Phys. Rev. Lett. **106**, 233201.

Weinberg, S., 1979, Physica **A96**, 327.

Weinberg, S., 1990, Phys. Lett. **B251**, 288.

Wildenthal, B., M. Curtin, and B. Brown, 1983, Phys. Rev. **C 28**, 1343.

Wilson, K., 1983, Rev. Mod. Phys. **55**, 583.

Wilson, K. G., 1971, Phys. Rev. **D 3**, 1818.

Witała, H., W. Glöckle, J. Golak, A. Nogga, H. Kamada, R. Skibiński, and J. Kuroś-Żołnierczuk, 2001, Phys. Rev. **C 63**, 024007.